Surface Enhanced Raman Scattering Enhancement Factors: A Comprehensive Study

E. C. Le Ru,* E. Blackie, M. Meyer, and P. G. Etchegoin†

The MacDiarmid Institute for Advanced Materials and Nanotechnology, School of Chemical and Physical Sciences, Victoria University of Wellington, PO Box 600, Wellington 6140, New Zealand

Received: December 21, 2006; In Final Form: July 17, 2007

This paper presents an in-depth study of Surface Enhanced Raman Scattering (SERS) enhancement factors (EFs) and cross-sections, including several issues often overlooked. In particular, various possible rigorous definitions of the SERS EFs are introduced and discussed in the context of SERS applications, such as analytical chemistry and single molecule SERS. These definitions highlight the importance of a careful characterization of the non-SERS cross-sections of the probes under consideration. This aspect is illustrated by experimental results for the non-SERS cross-sections of representative SERS probes along with average SERS EFs for the same probes. In addition, the accurate experimental determination of single molecule enhancement factors is tackled with two recently developed techniques, namely: bi-analyte SERS (BiASERS) and temperature-dependent SERS vibrational pumping. We demonstrate that SERS EFs as low as 10^7, as opposed to the figure of 10^{14} often claimed in the literature, are sufficient for the observation of single molecule SERS signals, with maximum single molecule EFs typically on the order of $\sim 10^{10}$.

I. Introduction

A. Historical Background. The "magnitude'' of the enhancement in surface enhanced Raman scattering (SERS) is an issue that has puzzled researchers right from its discovery. The initial conflict of understanding in the very first report of SERS[1] with respect to subsequent (more correct) interpretations[2,3] was precisely based on the "magnitude" of the effect and the difficulty in estimating the number of molecules that contribute to the signal. In effect, the first interpretation of SERS was based on the increased number of molecules that was postulated to exist on an electrochemically roughened (fractal like) substrate.[1] It became apparent afterward that the increase in signal was due to an increase in the apparent cross-section of the molecules, resulting in the concept of the SERS enhancement factor (EF).[2−4] This is part of the history of how SERS developed[4,5] and will not be reviewed here except for the purpose of highlighting the longstanding persistence of problems and misinterpretations surrounding the issues of the SERS cross-sections and the corresponding EFs. A reliable knowledge of the latter in different types of SERS active media has been a longstanding ambition of the SERS community.

There is an additional reason for properly characterizing SERS cross-sections and EFs: the single-molecule SERS problem. A bit more than 20 years after the initial discussions on the magnitude of the effect, the possibility of single-molecule (SM) Raman spectroscopy via SERS was proposed.[6,7] The question of the magnitude of the enhancement, and its physical origin, again came back to the center of the scene together with the uncertainty in the reality of the SM scenario itself. It is not an exaggeration to claim that part of the initial uncertainty in SM-SERS phenomena is strongly intertwined with the misunderstanding on the nature and magnitude of the enhancement. For example, it is often assumed that EFs on the order of 10^{14} are required for the observation of SM-SERS.[8] Because electromagnetic (EM) enhancements are believed to contribute, at most, to a factor $\sim 10^{10}$, an additional chemical enhancement must be invoked to "bridge the gap". One of the aims of this paper is to show that, provided the SERS EFs are correctly defined and measured, EFs on the order of 10^7-10^8 are, in fact, sufficient for the detection of SM-SERS signals. Moreover, it will also be shown that maximum SERS EFs are on the order of $\sim 10^{10}$ in typical SERS conditions and are at most on the order of $\sim 10^{12}$ in the best possible conditions (i.e., for large Ag colloidal clusters).

Arguably, the SERS enhancement factor is one of the most important numbers for characterizing the SERS effect. This is especially true for practical applications where the first concern is usually to know the magnitude of the enhancement factor that can be achieved. It is also an important figure when comparing with theoretical calculations. One criticism often heard is that SERS has not lived up to its original expectations, due to the inability to quantify the signals properly, and this is, of course, linked to the difficulty in measuring the EFs adequately. These issues have recently been emphasized by Natan in a lucid critical review of the current status of SERS.[9] Several studies have concentrated on rigorously measuring the SERS enhancement factors under specific conditions,[10−13] mostly focusing on average EFs. Average SERS EFs of the order of $\sim 10^4-10^6$ have been obtained, and sometimes as high as $\sim 10^8$ (depending on the definition and measurement procedure). However, most SERS practitioners will also be familiar with the fact that anything from 10^4 to 10^{14} may be quoted in the literature as SERS enhancements, in particular for (but not limited to) the SM-SERS problem. It is a fact that the EF can strongly depend on the exact SERS conditions: substrate, analyte, excitation wavelength, etc. However, the wide discrepancy in the quoted EFs also comes from the combined result of: (i) a wide variability in the definition of the EF, and (ii) the way it is estimated in practice. What the field is now lacking to further exploit these results is a detailed formal discussion of the possible definitions of the SERS EFs, including

* E-mail: Eric.LeRu@vuw.ac.nz.
† E-mail: Pablo.Etchegoin@vuw.ac.nz.

10.1021/jp0687908 CCC: $37.00
Published on Web 08/23/2007

those pertaining to SM detection. This is of crucial importance, both for a better fundamental understanding of SERS and for potential applications in analytical chemistry or SM spectroscopy. It seems that the time has come to attempt to rigorously and quantitatively address this issue in situations of interest for current research topics in SERS. The field is now in a mature position to approach this topic with the aid of recent developments, such as the use of nanolithography SERS substrates (for a better understanding of the enhancement mechanisms[11,13]), and more reliable tools to pin down single molecule SERS conditions (like the BiASERS method[14]). It is the purpose of this paper to develop new (and review existing) experimental and theoretical tools to address the SERS enhancement factor problem and to resolve longstanding contradictions and inconsistencies in the literature. We believe that such rigorous definitions and measurements of SERS EFs are crucial to the establishment of SERS as a practical analytical tool.

B. Overview. Because of the complexity of the subject, we heavily rely on the Supporting Information to the paper, where important aspects are explained in full detail for other authors to reproduce the numbers and use them in their own context. One such important aspect (often ignored) is, for example, the need to characterize the non-SERS properties of SERS analytes to obtain reliable SERS EFs. This will be discussed in full in Section S.III (Supporting Information). We also dedicate an extensive section (Section S.II, Supporting Information) to introduce and discuss a number of possible rigorous definitions of SERS EFs, whereas we only give their most important characteristics here in the main paper.

This paper mainly focuses on the presentation and discussion of the experimental measurements of the SERS enhancement factors. Accordingly, the SERS EFs definitions are only discussed briefly in Section II to set the framework (a lengthier and more general discussion is given in Section S.II, Supporting Information). In Section III, we tackle the issue of the experimental determination of average SERS EFs. The importance of the non-SERS cross-section measurements is highlighted in Section III, parts A and B (which are complemented by Section S.III, Supporting Information), whereas the actual results on the average SERS EFs are discussed in Section III, parts C and D. Section IV is devoted to the rigorous measurements of single molecule SERS EFs in various situations: (i) Ag colloidal solutions in Section IV, part B; (ii) dried Ag colloids (small clusters) in Section IV, part C; and (iii) large clusters of dried Ag colloids in Section IV, part D. These measurements require a careful characterization of the scattering volume, a subject treated in Section S.IV (Supporting Information). The bi-analyte[14] technique is used in Section IV, parts B and C, whereas temperature-dependent vibrational pumping is used in Section IV, part D (with additional details on this approach given in Section S.V, Supporting Information). Finally, the results are discussed in Section V, in particular, in relation to SM-SERS detection and to the presence/absence of a chemical contribution to the SERS EFs.

II. Different Definitions of EFs

We start the discussion with one of the main reasons for the disparity in the SERS EFs encountered in the literature, namely, the lack of rigorous definitions. This problem was in fact pinpointed recently by Natan[9] as one of four outstanding issues for SERS research and applications. We attempt to address this issue in this paper by proposing and discussing a number of possible definitions for the SERS EFs. We particularly emphasize three crucial points, which we feel have so far not drawn the attention they deserve: (i) the necessity of including the non-SERS properties (in particular Raman cross-sections) of the probes in the definition, (ii) the importance of distinguishing between EF definitions that are sensitive to the exact experimental conditions and to the SERS probe and those that are more intrinsic to the SERS substrate and therefore truly represent its performance, and (iii) the distinction between average SERS EFs and MF-SERS EFs; both are important characteristics of the substrate, but one or the other may be more relevant depending on the context or applications.

The diversity of situations that can arise in SERS, such as single molecules, multiple molecules, experimental limitations (i.e., not knowing the exact number of molecules), averages over time, spatial distribution, orientations of the probe on the surface, etc. make a single general definition of the EF impossible. By the same token, the number of possible definitions is commensurate with this complexity. To avoid the reader from being distracted with all the details, we only provide here in the main text the most important definitions and salient cases. Some of these cases are going to be illustrated explicitly in the experimental section. However, we do provide an in-depth discussion of all the different possible definitions of the enhancement factor in the Supporting Information, where we also provide additional definitions, not used explicitly in the experimental results of this paper.

With this in mind, we only briefly discuss three important and representative definitions.

A. The Single Molecule Enhancement Factor. This is the SERS enhancement felt by a given molecule at a specific point. It is, in general, dependent upon the Raman tensor of the probe and its orientation on the SERS substrate and with respect to the local field at that point. It is also dependent upon the orientation of the SERS substrate with respect to the incident laser polarization and direction. Hence, it requires the exact definition of the SERS substrate geometry and the exact position and orientation of the probe on it. Because of these constraints, this definition is much more suited to theoretical estimations of the EF, rather than experimental measurements.

To avoid conflicts with the orientation of the molecule (see Section S.II.B, Supporting Information), we introduce the definition of the single molecule enhancement factor (SMEF) as shown in eq 1;

$$\mathrm{SMEF} = \frac{I_{\mathrm{SERS}}^{\mathrm{SM}}}{\langle I_{\mathrm{RS}}^{\mathrm{SM}} \rangle} \tag{1}$$

where $I_{\mathrm{SERS}}^{\mathrm{SM}}$ is the SERS intensity of the SM under consideration, whereas $\langle I_{\mathrm{RS}}^{\mathrm{SM}} \rangle$ is the average Raman intensity per molecule for the same probe, also discussed extensively in Section S.III (Supporting Information). It can be shown that the SMEF defined in eq 1 can be expressed as a ratio of SERS over non-SERS differential cross-sections (see Section S.II.C of the Supporting Information for a discussion of the rigorous definition of the SERS cross-section).

$$\mathrm{SMEF} = \frac{\mathrm{d}\sigma_{\mathrm{SERS}}}{\mathrm{d}\Omega} \Big/ \frac{\mathrm{d}\sigma_{\mathrm{RS}}}{\mathrm{d}\Omega} \tag{2}$$

It can also be useful to define the orientation-averaged SMEF (OASMEF) at a given position as eq 3;

$$\mathrm{OASMEF} = [\mathrm{SMEF}] = \frac{[I_{\mathrm{SERS}}^{\mathrm{SM}}]}{\langle I_{\mathrm{RS}}^{\mathrm{SM}} \rangle} \tag{3}$$

where the average denoted by [...] is to be taken over all allowed orientations of the molecule in SERS conditions (not to be confused with the real orientation averaging denoted ⟨...⟩, because the orientation of the molecule on the surface can be hindered to a few specific cases only). Further properties of this definition are discussed in Section S.II.D (Supporting Information).

We note in passing that, in most cases, what is important is the maximum SMEF on a SERS substrate. This is particularly true for experiments where SM signals may only be detectable from the points of highest enhancements (hot-spots).

B. The SERS Substrate Point of View. For many SERS applications and experiments, the detailed distribution of the SMEF on the substrate, or even its maximum value, is irrelevant because one is mainly dealing with average SERS signals. It is, therefore, equally important to define one or more SERS substrate enhancement factors (SSEFs), which can be used to compare the average SERS enhancements across different substrates. In fact, most studies of SERS EFs, so far, have indeed focused on this aspect. The most widely used definition for the average SERS EF is eq 4:[10,11,13,15,16]

$$\mathrm{EF} = \frac{I_{\mathrm{SERS}}/N_{\mathrm{Surf}}}{I_{\mathrm{RS}}/N_{\mathrm{Vol}}} \tag{4}$$

where $N_{\mathrm{Vol}} = c_{\mathrm{RS}}V$ is the average number of molecules in the scattering volume (V) for the Raman (non-SERS) measurement, and N_{Surf} is the average number of adsorbed molecules in the scattering volume for the SERS experiments. This is normally taken as representative of a substrate. However, this definition presents a few problems (which are fully discussed in Section S.II.E, Supporting Information), and it is preferable to work with an alternative definition of a SSEF (eq 5);

$$\mathrm{SSEF} = \frac{1}{A_{\mathrm{M}}}\int_{A_{\mathrm{M}}} \mathrm{OASMEF(r)}\, \mathrm{d}S \tag{5}$$

where A_{M} represents the surface area of the metallic substrate. This last expression can be rewritten as eq 6;

$$\mathrm{SSEF} = \{\mathrm{OASMEF}\} = \{[\mathrm{SMEF}]\} \tag{6}$$

where {[SMEF]} is the spatial-and-allowed-orientation-averaged SMEF.

The SSEF can then be expressed in terms of the experimentally measured signals as eq 7:

$$\mathrm{SSEF} = \frac{I_{\mathrm{SERS}}/(\mu_{\mathrm{M}}\mu_{\mathrm{S}}A_{\mathrm{M}})}{I_{\mathrm{RS}}/(c_{\mathrm{RS}}H_{\mathrm{eff}})} \tag{7}$$

where c_{RS} is the concentration of the solution used for the non-SERS measurement, H_{eff} is the effective height of the scattering volume (see Section S.IV, Supporting Information), μ_{M} [m^{-2}] is the surface density of the individual nanostructures producing the enhancement, and μ_{S} [m^{-2}] is the surface density of molecules on the metal. This expression resembles the commonly used average EF given in eq 4, but with a rigorous definition of N_{Surf} and N_{Vol}, see Section S.II.E (Supporting Information) for more detail.

C. The Analytical Chemistry Point of View. The definitions introduced so far (SMEF and SSEF) have attempted to emphasize the intrinsic characteristics of the substrate and are not always straightforward for relating to experimental results. For many applications, however, one is mostly concerned with the simple question of how much more signal can be expected from SERS as compared to normal Raman under given experimental conditions. To address this question, we introduce another definition of the SERS EF, which is fairly intuitive and particularly relevant for analytical chemistry applications. Let us consider an analyte solution with concentration c_{RS}, which produces a Raman signal I_{RS} under non-SERS conditions. Under identical experimental conditions (laser wavelength, laser power, microscope objective or lenses, spectrometer, etc.), and for the same preparation conditions, the same analyte on a SERS substrate, with possibly different concentration (c_{SERS}), now gives a SERS signal I_{SERS}. The analytical enhancement factor (AEF) can then be defined as eq 8.

$$\mathrm{AEF} = \frac{I_{\mathrm{SERS}}/c_{\mathrm{SERS}}}{I_{\mathrm{RS}}/c_{\mathrm{RS}}} \tag{8}$$

This definition, although useful for specific practical applications, tends to strongly depend on many factors, in particular, on the adsorption properties and surface coverage (monolayer vs multilayer) of the probe; c_{SERS} does not fully characterize the number of adsorbed molecules. It is also strongly dependent upon the sample preparation procedure for 2D planar substrates (e.g., spin-coating, dipping, or drying). The AEF, in fact, ignores the fact that SERS is a type of surface spectroscopy, which means that only the adsorbed molecules contribute to the signal and that the effect is distance-dependent.[5,12] For this reason, it is not a good characterization of the SERS substrate itself, and it cannot be used to easily compare the performances of different substrates. However, provided all experimental procedures are clearly stated and submonolayer coverage is ensured, the AEF represents a simple figure for the SERS EF, whose measurement is easily reproducible. From its definition, it is also clear that the AEF is particularly suited to the case of SERS active liquids (e.g., colloidal solutions). Further details pertaining to the definition of the AEF are given in Section S.II.F (Supporting Information) and an explicit experimental example will be given in the next section.

D. Other Specialized Definitions of SERS EFs. In the Supporting Information we discuss, in addition, several other extensions of these definitions to accommodate other cases of practical interest (like modes with isotropic Raman tensors in which the SSEF or the SMEF do not depend on orientation averages). The definitions become more specific, and the best one to be used in each particular application should be selected carefully. The interested reader can find all of the additional definitions in Section S.II together with a summary in Table S.I (Supporting Information). We continue with an experimental implementation of some of these concepts.

III. An Experimental Illustration for Average SERS EFs

All the necessary definitions and elements to address the various aspects of SERS enhancement factors (EFs) are laid out in the previous sections and the corresponding Supporting Information. We now devote ourselves to one of the main motivations underlying this paper: the accurate experimental determination of SERS EFs and cross-sections. We first focus on experimental measurements of AEFs in colloidal solutions, which in addition illustrate the importance of the non-SERS characterization of the probes.

A. Experimental Measurements of Non-SERS Cross-Sections. As already pointed out, the first step when estimating SERS EFs, either theoretically or experimentally, is to consider the non-SERS case. This aspect has often been ignored in the past and is partly responsible for the unrealistically large

TABLE 1: Main Raman Active Modes of CV, RH6G, BTZ, and BTA, with Their Experimentally Determined Non-SERS Cross-Sections[a]

	$\bar{\nu}_i$ [cm^{-1}]	($d\sigma/d\Omega$) (non-SERS) [cm^2sr^{-1}]
CV	808	3.6×10^{-26}
	917	1.1
	1177[b]	6.1
	1200[b]	1.5
	1621	3.6
RH6G	612	0.67×10^{-27}
	774	0.76
	1185	0.60
	1311	1.0
	1364	1.8
	1510	2.4
	1652	1.0
BTZ	1108	1.0×10^{-28}
	1412	2.5
	1617	0.87
BTA	783	3.6×10^{-30}
	1019	4.7
	1376[b]	2.8
	1390[b]	2.8
	1599	1.3

[a] The absolute raman cross-sections are obtained by direct comparison, under the same experimental conditions, of integrated intensities to the 516 cm^{-1} mode of 2-bromo-2-methylpropane (2B2MP) with a reference cross-section of 5.4×10^{-30} cm^2/sr (see Section S.III, Supporting Information). [b] Peaks are part of a doublet.

enhancement factors sometimes reported in the literature. In ref 6 for example, the SERS EF for SM detection is estimated to be around $\sim 10^{14}$, on the basis of a SERS measurement of the dye crystal violet (CV) as compared to reference non-SERS values of methanol under the same experimental conditions. It is well-known that dyes can have Raman cross-sections of up to 10^6 times larger than smaller molecules, especially in Resonance Raman Scattering (RRS) conditions.[5,17] What is often less appreciated is that such dyes still have large Raman cross-sections even in non-resonance conditions because of preresonance effects (as will be shown here). This means that one cannot "guess" the non-SERS cross-section and then use it to estimate the SERS EFs. Such an approach is one of the causes for the apparently enormous EFs of $\sim 10^{14}$ frequently quoted in the literature. Therefore, the non-SERS cross-section must either be calculated from first-principles, such as in ref 17, or if possible, measured experimentally (if the Raman signals are not completely engulfed by fluorescence).

To measure the SERS EFs, it is usually not necessary to know the absolute cross-section of the analyte; a measurement of relative intensities can be enough. However, measuring the non-SERS cross-section of common SERS analytes is useful for several reasons; (i) it avoids having to make non-SERS measurements (which usually involves high-concentration samples and long integration times) each time a SERS EF is sought, (ii) it highlights the fact that some non-resonant dyes can still have a larger-than-expected non-SERS cross-section, (i.e., preresonance effects are in general much more common than generally assumed), and (iii) it shows that, effectively, different analytes can have widely different intrinsic non-SERS cross-sections as a starting point, which can differ by several orders of magnitude in some cases. These latter two aspects will be illustrated in this section by measuring the non-SERS cross-sections of four representative SERS analytes at 633 nm laser excitation, namely; (i) CV, a dye that absorbs strongly with a maximum at 590 nm and is, accordingly, close to a RRS condition; (ii) rhodamine 6G (RH6G), another dye, which has its maximum of absorption at 528 nm and, a priori, could therefore be considered as non-resonant; (iii) a benzotriazole dye (3-methoxy-4-(5′-azobenzotriazolyl)phenylamine, dye #2 of ref 18, denoted BTZ here), a smaller dye with absorption close to the UV ($\approx$400 nm) and therefore even further from resonance at 633 nm; and (iv) benzotriazole (BTA), a smaller compound with a single aromatic ring, absorbing in the UV and therefore non-resonant.

These compounds are typically good SERS analytes, because they tend to adsorb efficiently on gold and silver surfaces. BTZ and BTA are believed to adsorb covalently to Ag through the triazole group.[18] CV and RH6G have, in fact, appeared in a large proportion of the SERS studies in the literature. It is sometimes assumed that Raman spectra from resonant dyes are difficult to obtain because of the overwhelming fluorescent background. At 633 nm, this was indeed the case in our experiments for other dyes such as methylene blue and nile blue (NB). However, this problem can be avoided in at least two situations: (i) for non-resonant dyes (for example BTZ) or dyes in preresonance conditions (for example, RH6G at 633 nm), and (ii) for resonant dyes with a very fast nonradiative decay (which drastically reduces the fluorescence quantum yield). For example, CV has such a fast nonradiative channel because of fast rotation-isomerization of the arms of the structure around the central carbon atom. For this reason, measurements of Raman signals are possible in CV even under nearly-resonant excitation.

The compound 2-bromo-2-methylpropane (2B2MP) was used as a reference for all non-SERS cross-sections measurements. Full experimental details and Raman spectra are given in Section S.III, Supporting Information. The measured absolute Raman cross-sections for the main Raman peaks of these four compounds are summarized in Table 1.

B. Discussion of Non-SERS Cross-Sections. The first obvious remark is that these cross-sections span a range of 4 orders of magnitude and can be much larger than typical Raman cross-sections. This is, in part, because of the relatively large size of these molecules but above all is because of resonance or preresonance Raman effects. The near-resonant condition for CV is reflected in the large cross-sections, which are, in fact, not surprising and typical of RRS cross-sections. For example, the cross-section of RH6G at resonance was recently predicted[17] to be on the order of 10^{-25} cm^2/sr. For RH6G, whose absorption peaks at 528 nm and is negligible at 633 nm, a clear preresonance effect is still evident. The large cross-sections of RH6G highlight the important fact that even non-resonant molecules can have fairly large cross-sections because of preresonance effects. These effects are present even for BTZ, whose absorption is even further away from excitation and would by most standards be considered non-resonant. The non-resonant nature of the Raman effect cannot therefore be guessed simply from the absorption properties of the probe.

Moreover, as a point of comparison, the Raman cross-section of the 1033 cm^{-1} mode of methanol (used in the past as a reference for SERS EF estimations[6]) is only on the order of 1.8×10^{-31} cm^2/sr at 633 nm. This corresponds to between 30 (for BTA) or 3×10^5 (for CV) times smaller than the cross-sections measured here. These large non-SERS cross-sections mean that such molecules can, in principle, be observed in SM-SERS experiments with SERS EFs much less than those usually claimed. We will show in the next section that SERS EFs on the order of $\sim 10^7 - 10^8$ are, in fact, in most cases sufficient. This is 6−7 orders of magnitude smaller than what has been claimed for many years in the literature.[6,8] We will also show

that even in the best possible conditions, the maximum SERS EF is at most on the order of 10^{12}.

In summary, all of the elements for a reliable characterization of the non-SERS Raman cross-sections of typical SERS probes have been given (see Section S.III of the Supporting Information). The compound 2B2MP appears as a reliable reference compound for future comparisons among data. The two common SERS dyes tested here (RH6G and CV) exhibit (due to resonance or preresonance effects) non-SERS cross-sections at 633 nm that are much higher than what may be assumed a priori. This implies that single molecule SERS conditions can be achieved for these dyes at much smaller EFs than the enormous values ($\sim 10^{14}$) quoted frequently in the literature, as will be further confirmed later.

C. Experimental Measurements of Analytical EFs. We now consider the average SERS EFs obtained from an analyte in a (partially aggregated) Lee and Meisel Ag colloid solution.[19] The neat colloid solution is pushed close to (but below) the critical aggregation condition by the addition of salt (KCl), following previous studies on the same system.[20] For the specific case at hand, it implies mixing the colloidal solution with a 20 mM KCl solution in a 50%/50% proportion (thus achieving a 10 mM KCl concentration in the final sample). The long-term stability and characteristic clusters present in this system have been studied elsewhere.[20] A small volume of the SERS probe is then added to obtain the required concentrations. At sufficiently low analyte concentrations ($\leq$100 nM) the stability of the colloids close to the aggregation limit is not affected by the additional screening of the repulsive potential introduced by the analytes. The SERS experiments were carried out for dye concentrations of 5 nM (which implies an estimated 60 dyes per colloid[14] or one molecule per $\sim$200 nm^2 on the surface). For the other probes, a maximum concentration of 1 μM was used (for BTA). In all cases, these concentrations are well below monolayer coverage, which excludes any influence of multilayer effects on the results. The AEF can be directly obtained from its definition, eq 8. The measurements were carried out with a $\times$100 water immersion objective, for which the scattering volume is relatively small. Long acquisition times are therefore required (minimum 10 min) to average over all cluster types/geometries and, therefore, to eliminate the influence of any fluctuations of the SERS signals. Moreover, in practice, we do not directly compare the SERS and the non-SERS intensities, which would be cumbersome (this would imply using a large analyte concentration, which would then require a thorough cleaning of the objective). Instead, the SERS intensity is compared to the reference compound 2B2MP and an average (apparent) absolute differential cross-section is deduced. This is then compared to the absolute cross-section in the non-SERS case (measured using the same reference compound).

Table 2 is a summary of the results obtained for the four analytes already studied here: RH6G, CV, BTZ (dye 2 of ref 18), and BTA. Note that the AEFs quoted in this table are specific to the exact preparation conditions of the SERS solution (which was the same for the four analytes). Adding less or more KCl to the Ag colloids would affect the AEFs; this is normal because we are then not dealing with the same SERS substrate.

D. Discussion of the Analytical EFs. These figures suggest a number of interesting and important remarks.

• The AEFs are on the same order of magnitude for all four compounds, suggesting that any form of probe-dependent enhancement (such as chemical enhancement, CE) does not play a significant role for these probes (or, alternatively, it is similar in magnitude for all four, an unlikely coincidence). In fact, the small variations in AEFs can simply be attributed to electromagnetic effects and surface selection rules as discussed below.

TABLE 2: Main Raman Active Modes of RH6G, CV, BTZ, and BTA, with Their Experimentally Determined Non-SERS and SERS Frequencies[a]

	$\bar{\nu}_i$ (Raman) [cm^{-1}]	$\bar{\nu}_i$ (SERS) [cm^{-1}]	AEF
RH6G, 5 nM	612	612	5.0×10^5
	774	768−778[b]	4.2
	1185	1181 (1198)[b]	4.5
	1311	1312 (1292)[b]	4.4
	1364	1363 (1349)[b]	3.4
	1510	1511	3.4
	1652	1651	3.1
CV, 5 nM	808	804	1.0×10^5
	917	914	1.8
	1177 (1200)[b]	1176	0.53
	1621	1622	0.86
BTZ, 100 nM	1108	1106 (1125)[b]	6.4×10^5
	1412	1390 (1413)[b]	6.2
	1617	1616	8.2
BTA, 1 μM	783	787	3.5×10^5
	1019	1035 (1021)[b]	4.5
	1376−1390[b]	1369−1394[b]	5.4
	1599	1579	7.8

[a] The concentration for the SERS experiments is given in the first column. [b]Peaks are part of a doublet. For each mode of each molecule, the AEF corresponds to that measured for the same Ag colloidal solution prepared as detailed in the text.

• These figures also demonstrates the importance of a proper characterization of the non-SERS cross-sections for the measurement of SERS EFs. By simply comparing the SERS intensities at the same nominal concentration, one observes that CV exhibits a much greater SERS signal than the others and may conclude its SERS EF is larger. Once normalized to the non-SERS cross-section, the appropriate EFs are obtained. The apparent strength of the CV SERS signals at 633 nm comes purely from a resonance contribution to the total intensity, which was already present in the non-SERS case.

• These enhancements are relatively low compared to some EFs encountered in the literature, simply because they are average EFs. As will be shown later, the observed SERS signal actually originates from a small subensemble of molecules (those located at hot-spots), experiencing much higher enhancements. If one could position all the molecules at these hot-spots, then much larger average enhancements could be obtained. This is a demonstration of how the issue of spatial averaging affects the definition and magnitude of what we understand as a specific type of EF.

• It is interesting to dwell on the relative peak intensities in SERS conditions. Note that by definition of the AEF, the changes in relative peak intensities from Raman to SERS are directly reflected in the variations of the AEFs from peak to peak. If the AEFs of all modes for a given probe are equal, then the relative Raman peak intensities are unchanged in SERS. Let us first consider the case of RH6G. As seen in Table 2, there is a clear trend for a slight decrease of the AEFs with mode energy. This can be simply explained within the EM theory of SERS. The EM EFs in SERS have two multiplicative contributions from the underlying plasmon resonance, one at the laser wavelength and one at the Stokes wavelength.[11,13,21,22] Because of the finite spectral width of the plasmon resonance, it is not possible to simultaneously fulfill both resonance conditions to the same degree, especially for large Stokes shifts. This is a well-known effect in SERS, and is the reason why hydrogen stretching modes around 3000 cm^{-1} tend to be weaker

under SERS conditions.[5] It can be shown that the EF is typically a factor of $\sim$1.4−3 smaller for modes around 1600 cm^{-1} as compared to the low-energy modes. This is similar to what is experimentally observed here for RH6G. The fact that this small effect is observable for RH6G must also mean that the vibrational modes (Raman tensors) are not much modified by adsorption onto Ag, and that the surface selection rules[23] do not play an important role here. The former assertion is further confirmed by the negligible changes observed in most peak frequencies from normal Raman conditions to SERS. The latter could be explained if the adsorption geometry is random or if the modes have similar symmetries (imposed by the preresonance Raman effect).

• The same trend is not observed for BTZ and BTA, but the AEFs can then be explained by a fixed adsorption geometry, which amplifies the effect of surface selection rules.[23] To illustrate this, we focus on the case of BTA. Adsorption is believed to occur through the formation of a covalent bond between Ag and a N atom of the triazole group.[24,25] Let us assume that the benzene ring extends out of the metal surface and that the molecular long axis is therefore perpendicular to the metal and aligned with the local field. Raman modes with a large component along this axis are then favored as compared to other modes. It is possible to show that the Raman tensors of the modes of BTA obtained from DFT calculations (not shown here) are compatible with the observed AEFs. For example, the 1599 cm^{-1} of BTA is strongly uniaxial along the long molecular axis (whereas the other modes considered here are more isotropic). This is consistent with the larger AEF observed for this mode.

• Finally, the case of CV is more difficult to interpret. First, the AEFs are markedly smaller than for the other molecules, by a factor of 3−10, depending on the mode. Such a factor is probably too large to be a result of surface selection rules. This could be attributed to a chemical contribution (quenching in this case), but we will show later that under different conditions the same SERS EFs are measured for CV and RH6G. We therefore attribute this decrease to either a reduced adsorption efficiency of CV on Ag colloids or to photobleaching; both effects would reduce the AEF. The remaining variations in the relative peak intensities (relative AEFs) can then be attributed to surface selection rules. Additional measurements with a similar compound (malachite green) not shown here demonstrate the drastic effect that photobleaching can have on the estimation of AEFs. Malachite green is resonant at 633 nm but with a markedly lower photostability than CV. AEFs are reduced even further in this latter case. A meaningful comparison among AEFs for different compounds in a given SERS substrate can only be made if photobleaching plays a minor or negligible role and adsorption efficiencies are comparable.

We conclude from these series of results that: (i) there does not seem to be any chemical contribution (or at least all the results can be explained from the EM theory of SERS) to the SERS EFs for the four molecules considered here, despite the fact that molecules like BTZ and BTA are believed to adsorb covalently on Ag; and (ii) the EM AEF for the low-energy modes for this colloidal solution is on the order $\sim 5 \times 10^5$. This gives a yardstick order of magnitude for the analytical enhancement factor at low concentrations in Lee and Meisel colloids, which should be easily reproducible by independent studies, provided the same preparation procedure is used.

A final comment on the results of colloidal solutions is that it is more difficult (and possibly less useful in this context) to estimate the SSEF for colloidal solutions, because the SSEF refers to a fixed substrate geometry. In a colloidal solution, the SERS substrate geometry is not fixed but is constantly changing through Brownian motion and diffusion of clusters in the scattering volume of the immersion objective. The orientation of the clusters/colloids with respect to the incident polarization is also constantly changing. The AEF measured here is therefore an average over all types of clusters present in the solution of the individual polarization-averaged SSEFs (PASSEF, see Section S.II, Supporting Information). The SSEF of an individual cluster is therefore difficult to measure, but the variations of SSEF from cluster to cluster manifest themselves experimentally in the form of the SERS intensity fluctuations, observed on a short time-scale (50−100 ms) as individual clusters diffuse through the scattering volume.

IV. Single Molecule Enhancement Factors

We now provide several examples of the experimental determination of SM-SERS EFs. We will, in particular, focus on the dye RH6G, one of the most widely used probes in SERS. We again focus exclusively on the 633 nm excitation, for which the non-SERS properties have been fully characterized.

A. Preliminary Considerations. It is a more difficult undertaking, in general, to estimate the SMEF (as compared to the Analytical EF) and a number of assumptions must be made to that end. There are, in particular, several issues to consider.

• It is difficult to make sure that a given SERS signal indeed originates from a single molecule, as opposed to a few or many. Reducing the dye concentration is an option but still presents a number of problems. In particular, the number of single molecule events decreases drastically, as discussed extensively in previous papers.[14,26] The best approach, in our opinion, is the use of the two-analyte technique (BiASERS), developed in ref 14. This technique, combined with relatively low (but not ultralow) concentrations offers a compromise whereby a large number of SM events can be obtained together with an easy way of identifying them (by rejecting multimolecules events).

• In a typical BiASERS experiment, one can identify many SM events, with varying intensities. This simply reflects the wide range of SMEFs that are normally encountered for most types of SERS substrates. The observed intensity (and therefore SMEF) depends on many parameters, including whether the molecule is exactly at the hot-spot or is slightly displaced, whether the excitation is at exact resonance or not, whether the incident polarization is optimally coupled to the hot-spot axis, etc. As a consequence, a wide range of SMEFs can be measured in a given sample. The observed events do not have a unique value for the EFs but rather span over a range of values where single molecule SERS signals are visible. What is, in general, interesting is the maximum SMEF achievable, and this can be measured by selecting the SM events with the largest intensities in the BiASERS technique. Provided that sufficiently many SM events are sampled, the strongest one must then correspond to those for which all parameters (molecule position, plasmon resonance, and polarization) are optimal. In the following we will focus, in particular, on measuring this maximum SMEF.

• To extract an absolute Raman cross-section and a corresponding SMEF from a SM-SERS event, it is necessary to accurately characterize the scattering volume of the Raman system. Rough estimates of the scattering volume are commonplace in the literature, but a rigorous determination of the SMEF requires a characterization that is as accurate as possible. The difference between a rough and a careful characterization of the scattering volume could mean an order of magnitude in the final result for the enhancement factor. We therefore devote

an extensive discussion in Section S.IV (Supporting Information) to this important aspect. The reader interested in the technical aspects of the scattering volume characterization for the estimation of SMEFs should refer to the Supporting Information provided.

These issues, even when addressed as thoroughly as possible, may still contribute to some uncertainty in the exact SMEF, possibly by a factor of ~2. Such an accuracy is, however, sufficient for comparison of most SERS substrates or SERS probes, and it represents an unprecedented degree of accuracy as compared to the many-orders-of-magnitude spread found in the different claims in the literature.

B. SMEF in Ag Colloidal Solutions. The SERS colloidal solution consisting of Lee and Meisel Ag colloids[19] with KCl was prepared as in the AEF experiments of Section III, part C. We propose to estimate the maximum SMEF of RH6G for this SERS solution. To do so, we prepare three solutions; one has a final concentration (c_{SERS}) of 1 nM of RH6G, one has 1 nM of NB, and a third one where a mixture of NB and RH6G is added to a final concentration of 1 nM for each dye. The presence of two different dyes in the latter enables us to test for the presence of SM-SERS signals.[14] The NB dye was selected as a BiASERS "partner" for RH6G because they can easily be distinguished through their well-defined low-energy peaks at 612 cm^{-1} for RH6G and 590 cm^{-1} for NB. We shall, therefore, mostly focus on the SMEF for the 612 cm^{-1} mode of RH6G at 633 nm. The SMEF for NB cannot be calculated here (only its SERS cross-section) because it was not possible to characterize its non-SERS properties because of the overwhelming fluorescence background at 633 nm excitation. In other words, NB is only being used here as a tool to "distinguish" RH6G SM events. We use the ×100 water immersion objective for excitation and collection at 633 nm. The incident power was 4.4 mW at the sample, which corresponds to a maximum excitation density of 7×10^5 W cm^{-2} at the center of the beam.

Following the arguments in ref 14, we can isolate single SERS spectra from the mixed sample, acquired over a short integration time (0.05 s here) where the signal of one dye or the other is completely absent. We refer to these spectra as SM-SERS events. For the concentrations used here, we estimate that there are approximately 12 molecules of each type per colloid. However, the surface area of a hot-spot is typically much smaller than that of the neighboring metallic surfaces,[14,26] typically 1% at most. Hence, the chance of a molecule adsorbing at a hot-spot are small, less than 1 in 10. Such hot-spots are formed in colloidal aggregates, which may therefore contain several hot-spots, increasing the chances of observing a SM-event. In addition, some aggregates are likely not to be optimally resonant, and no signal should be observed for these, even when a molecule is present at a hot-spot. These considerations are reflected in the observed statistics of SERS signals. Out of 2000 successive spectra, only about 1 in 20 exhibits a detectable SERS signal. These were analyzed by fitting the 612 cm^{-1} RH6G peak and the 590 cm^{-1} NB peak to determine their intensities. These intensities were then transformed into an apparent cross-section using the arguments of Section S.IV (Supporting Information). The results are plotted in Figure 1. Among these events, we can easily identify SM-SERS events for RH6G and for NB. For these SM events, the apparent cross-section of the event is then equal to the SM-SERS cross-section. Using the non-SERS cross-section of the RH6G 612 cm^{-1} mode (6.7×10^{-28} cm^2/sr, see Section III, part A), we then deduce the corresponding SMEF for some of the RH6G SM-SERS events (see Figure 1).

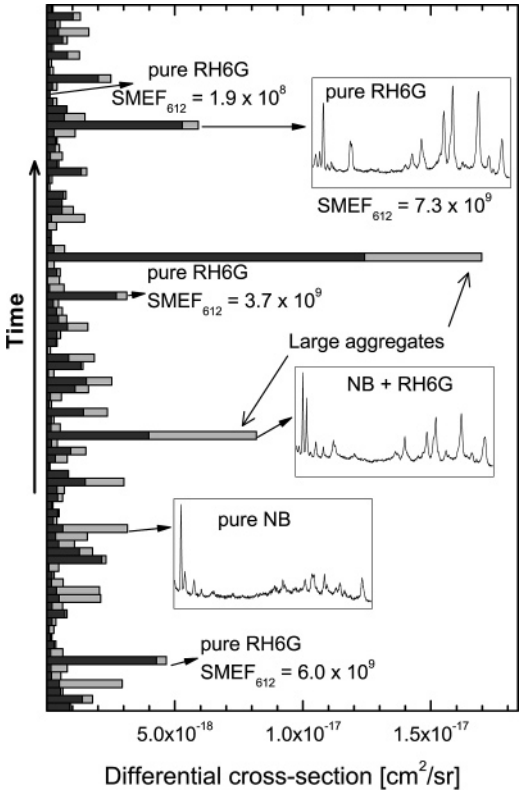

Figure 1. Analysis of the BiASERS experiment with RH6G and NB in a Ag colloidal solution. Each event on the vertical axis corresponds to an individual SERS spectrum (0.05 s integration time). The apparent absolute differential cross-section of the 612 cm^{-1} mode of RH6G (dark gray) and of the 590 cm^{-1} mode of NB (light gray) are shown as (cumulative) bars on the *x*-axis. Examples of SERS spectra (over the full range of acquisition, from 550 cm^{-1} to 1700 cm^{-1}) are given for pure SM-SERS RH6G and NB events, and also for a mixed event. The SMEF of the 612 cm^{-1} mode of RH6G is also given for a few selected SM-SERS RH6G events. The two large mixed events are attributed to large colloidal aggregates, as discussed in the text.

It is interesting that the strongest events in Figure 1 are of a mixed type (not SM-SERS), and this is generally observed in other similar experiments. Such intense mixed events can be attributed to large aggregates, which contain many hot-spots. The BiASERS approach is crucial here for identifying these events and excluding them from the analysis. One minor drawback, however, is that the SMEF for a given hot-spot in these large clusters (which could be expected to be larger than for the smaller cluster showing SM signals) cannot be determined within this approach. We shall come back to this aspect later when discussing temperature-dependent vibrational pumping.

From these results and several other similar experiments, we conclude that the maximum SMEF for the 612 cm^{-1} mode of RH6G achievable for this Ag colloidal solution (for our preparation procedure) is in the range $5-8 \times 10^9$, which corresponds to SERS differential cross-sections of $3-5 \times 10^{-18}$ cm^2/sr. These figures are many orders of magnitude smaller than what is usually assumed to be necessary. Moreover, for such SMEFs, the signals are still much larger than the detection limit of our system, despite the fairly short integration time of only 0.05 s. In fact, SM detection is possible with a much smaller SMEF, as low as 1.9×10^8 in our case, corresponding to a SERS cross-section of 1.3×10^{-20} cm^2/sr (i.e., the small RH6G SM-SERS event at the top of Figure 1). This figure could, in fact, be even smaller with longer integration times, around only 10^7 for the SMEF and less than 10^{-21} cm^2/sr for the cross-

section for a typical integration time of ~1 s. We believe these figures to be the most rigorous values for SMEFs ever reported to date, and they show that claims of EFs on the order of $\sim 10^{14}$ to see single molecules are primarily based on a misconception and a "loose" definition of the EF together with a neglect of the original non-SERS cross-section with all of its contributions from resonance or preresonance effects. Enhancement factors that are 6−7 orders of magnitude smaller than those from "loose" definitions are, in fact, enough to observe single molecules.

C. SMEF for Fixed Colloidal Structures. As another example of the use of BiASERS to determine SMEFs, we now study the case of colloidal aggregates fixed onto a substrate. A solution was prepared as in the previous section, but with a 15 mM final KCl concentration instead of 10 mM. The solution in this case is no longer stable and becomes clear within a few hours. Before this collapse, we dried a 20 μL drop onto a silicon substrate previously coated with a thin layer of poly-L-lysine. This forms a film of isolated colloidal aggregates, strongly attached to the substrate through electrostatic attraction (poly-L-lysine is positively charged). The SERS experiments is then carried out in liquid (using a drop of water) with the same ×100 immersion objective as before. Because the substrate is now fixed, we can use a longer integration time (1 s in our case), but the dyes are then more likely to exhibit photobleaching. We therefore decrease the power to 0.044 mW (100 times smaller). The RH6G SERS SM signals are then stable over minutes, and a small hint of photobleaching is still observed for NB. We acquired a series of SERS spectra by scanning along a line with a 0.2 μm step. The signals were analyzed as described in the previous section, and the results are presented in Figure 2.

The results are similar to those obtained for colloidal solutions, with a few differences worth pointing out. The SM-SERS cross-section for the 590 cm^{-1} mode of NB appears to be much larger than the one observed in the previous section. We attribute this to photobleaching effects. Because a small amount of NB photobleaching is evident here, even for a power density reduced by a factor of 100, it is likely that, in the previous experiment at full power, the NB molecules that experience the largest EF photobleach much faster than the integration time of 0.05 s, thereby reducing the measured cross-section. This effect highlights the importance of a careful choice of the probe and experimental conditions when estimating and comparing SERS EFs, especially regarding the photostability of dyes. Another aspect for fixed colloidal substrates is the lack of statistics. In one line scan we probed only ~10 aggregates, as seen in Figure 2, whereas in the same time we could acquire ≈1000 spectra of individual aggregates in solution thanks to the intrinsic Brownian motion. This lack of statistics makes it very difficult to determine the reliably of the maximum achievable SMEF. It appears that the RH6G SMEFs obtained in Figure 2 are comparable with those of Figure 1, but those of Figure 1 are more statistically sound. Note that this would not be an issue for more regular/ordered SERS substrates, such as those fabricated by nanolithography.

D. Measuring the SMEF Using Temperature-Dependent Vibrational Pumping. Finally, before discussing these results, we present an additional measurement of SMEFs using an alternative technique, namely temperature-dependent vibrational pumping (TDVP). The use of SERS vibrational pumping to determine SERS cross-sections was proposed more than 10 years ago[27] but has been the subject of much controversy[28,29] because, among other things, of the difficulties in experimentally distinguishing between pumping and heating effects.[30−32] Recent developments[33,34] have shown that these can be avoided by monitoring the temperature dependence of the anti-Stokes to Stokes ratio down to low temperatures (typically ~77 K or less). The exact meaning of the measured cross-section, called the pumping cross-section, has also been studied and discussed; see ref 33 for details. The pumping approach is complementary to the BiASERS technique used here for a number of reasons: (i) First, as shown in ref 33, it automatically yields an estimate of the maximum achievable SMEF on the SERS substrate and thereby avoids most of the problems associated with the lack of statistics. (ii) In addition, as pointed out earlier, the largest aggregates always contain many hot-spots and therefore tend to be excluded from the BiASERS analysis. The SMEF at a hot-spot in a large cluster cannot, therefore, be measured with BiASERS. We will use TDVP to attempt to measure the SMEF in such large Ag colloid clusters. To this end, the Ag colloid sample is prepared in a strongly aggregated state (as opposed to a partially aggregated state as before) by using large analyte concentrations (1 μM).[33] (iii) Finally, the TDVP does not require comparison to a reference for the cross-section estimation. Therefore, it does not need a careful characterization of the scattering volume but only of the excitation profile. The figures obtained are, therefore, entirely independent of those obtained using BiASERS.

However, this approach is still under development, and a number of approximations, not all of them yet rigorously

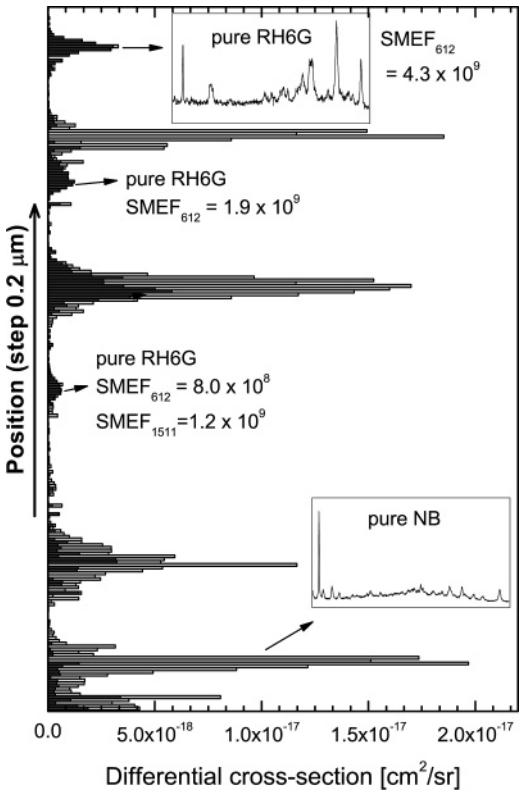

Figure 2. Analysis of the BiASERS experiment with RH6G and NB for fixed Ag colloidal aggregates on a silicon substrate and immersed in water. Each event on the vertical axis correspond to an individual SERS spectrum along the line scan (0.2 μm steps). The apparent absolute differential cross-section of the 612 cm^{-1} mode of RH6G (dark gray) and of the 590 cm^{-1} mode of NB (light gray) are shown as (cumulative) bars on the *x*-axis. Examples of SERS spectra (over the full range of acquisition, from 550 cm^{-1} to 1700 cm^{-1}) are given for pure SM-SERS RH6G and NB events. The SMEF of the 612 cm^{-1} (and 1511 cm^{-1} in one case) mode of RH6G is also given for a few selected SM-SERS RH6G events.

TABLE 3: Summary of the TDVP Results for RH6G and CV[a]

	$\bar{\nu}_i$ (SERS) [cm^{-1}]	σ_{pump} [cm^2]	$(d\sigma_{SERS}/d\Omega)$ [cm^{2}sr^{-1}]	$SMEF_{Max}$
RH6G	612	2.1×10^{-15}	0.50×10^{-15}	7.5×10^{11}
	1363[b]	5.0	1.2	6.6
	1511	7.7	1.8	7.6
	1651	3.7	0.88	8.8
CV	804	7.8×10^{-14}	1.9×10^{-14}	5.2×10^{11}
	914	3.2	0.76	6.9
	1176	10	2.4	3.9
	1622	8.8	2.1	5.8

[a] The pumping cross-sections (σ_{pump}) are derived from a fit to the data as described in ref 33. The maximum differential SM-SERS cross-section $(d\sigma_{SERS})/(d\Omega)$ and the maximum SMEF on the substrate are then obtained as detailed in Section S.V (Supporting Information). Note that the maximum SMEF is similar for both molecules. [b]Peaks are part of a doublet.

justified, have to be made to extract the SMEF. The most salient of approximations is the estimation of the vibrational lifetime of the mode.[33] The results must therefore be taken with those provisos in mind, but we feel, nevertheless, that they add another dimension to the SMEF problem, which is why we present them in this paper as a complementary estimation.

We focus here on two analytes, RH6G and CV, at 633 nm. The details of the experimental procedure, results, and analysis to extract the SMEF are given in Section S.V (Supporting Information). As explained there, the maximum SMEF available on the sample can be deduced, taking into account the non-SERS cross-sections derived earlier. These maximum SMEFs are summarized in Table 3 for representative modes of RH6G and CV.

These figures show that the maximum SMEF on these large Ag-colloid clusters is on the order of $7-8 \times 10^{11}$. It is interesting to note that the same SMEF is obtained for RH6G and CV (except for small factors (<2) attributed to surface selection rules). Again, this strongly suggests that there is no chemical contribution to the SERS enhancement in this case (or it is of the same magnitude for both dyes; an unlikely coincidence). Moreover, the SMEF derived here is around 2 orders of magnitude larger than that obtained using the BiASERS approach for small clusters. This difference comes from the different nature of the SERS substrate. Within the BiASERS approach, we only probe small- or medium-sized clusters. Large clusters are automatically excluded from the analysis because they generally exhibit signals from many molecules. This problem can be overcome using the TDVP approach. The SMEF derived here ($7-8 \times 10^{11}$) corresponds to the maximum achievable SMEF on Ag (the most SERS-enhancing metal) colloids, in their most aggregated state (i.e., these are the most favorable conditions to large SERS enhancements). Therefore, we believe it should be viewed as the upper limit of what is achievable with SERS. This upper limit is still at least 2 orders of magnitude smaller than the "conventional" EFs of 10^{14} assumed many times in the past.[8]

V. Discussion and Conclusions

It is interesting to note that the approaches of vibrational pumping and BiASERS bring a contribution to the same problem and a portion to its answer, but from two different ends. Temperature-dependent vibrational pumping[33,34] is capable of measuring the SERS cross-section independently of the number of molecules by introducing a "nonlinearity" to the anti-Stokes signal (the pumping term) and providing a measure that is self-normalizing with respect to the number of molecules. The SM approach, epitomized by the BiASERS technique, on the other hand, resolves the same issue in a completely different manner; what is known now is the number of molecules producing the signals. If the signal is compared to a reference sample with a known number of molecules and a known cross-section then the SMEF follows immediately. The intermediate step of characterizing the normal (non-SERS) cross-section is always mandatory.

The values obtained for the SERS enhancement factors in this paper deserve a few additional comments:

In colloidal solutions, the largest measured SMEF is on the order of 7×10^9. This SMEF is, therefore, about 10^4 times larger than the AEF measured in the same conditions. This apparent discrepancy has at least two causes. The main origin is the high nonuniformity of the EF distribution.[26] Large EFs occur only at very localized positions (hot-spots), and this is the EF that is measured by the SMEF (largest EF on the substrate). The average EF has been predicted to be 250−500 times smaller than the maximum EF,[26] so it is expected that the SSEF is 250−500 times smaller than the SMEF. The additional factor of 20−30 between the SSEF and the AEF can be attributed to the polydispersity of colloidal clusters (and therefore of their resonance conditions) and to polarization averaging. The resonance condition and orientation of the cluster in the scattering volume constantly changes. The optimum coupling is automatically selected when the largest SM events are observed, but averaging over all orientations and resonance conditions results in the observed decrease of the average EF when measuring the AEF.

Moreover, our results show that SERS from a single molecule can be observed with an integration time of only 0.05 s and with a differential SERS cross-section of only $\approx 10^{-20}$ cm^2/sr. This is at least 4 orders of magnitude smaller than what is usually assumed to be necessary in the literature. The reason for this discrepancy is that these previous estimates were usually based on the requirements of SM-fluorescence. In this case, the signal is much wider, typically 500−1000 cm^{-1} as compared to only $\approx$6 cm^{-1} for the SERS peak of RH6G considered here. This narrowing by a factor $\approx$100 allows the detection of signals whose integrated intensity is $\approx$100 times weaker. Another effect contributing to this discrepancy is the fact that single molecules in solution diffuse much faster than typical colloids, and integration times in SM-fluorescence are therefore much smaller than what is allowed for SERS. This can easily account for another factor of 100 in the detection limit of single molecules. These two important aspects of SM-SERS, narrower peaks and longer diffusion times (or even fixed molecules on fixed substrates), have been largely ignored so far, but they do mean that SM-SERS is possible with cross-sections at least 4 orders of magnitude lower than for typical SM-fluorescence. In fact, a cross-section as low as 10^{-21} cm^2/sr is sufficient to observe SERS from a single molecule with an integration time of 1 s. This corresponds to a SMEF of only 10^7 for RH6G at 633 nm. For a more resonant molecule, such as CV at 633 nm or RH6G at 514 nm, a SMEF as low as 10^5 may even be sufficient for SM-SERS (if photobleaching is not an issue). This is 9 orders of magnitude smaller than what is typically assumed.[8]

We believe the results of this paper settle a matter that has been around for a decade since the initial proposal of SM sensitivity in SERS,[6,7] namely, how much enhancement is needed to observe a SM in SERS? With the benefit of hindsight, we see that the abnormally large enhancements that were proposed in some of the original reports are the natural consequence of several facts, the most important of which are:

(i) an ill-defined EF, where the necessary normalization with respect to non-SERS conditions was sometimes completely ignored; (ii) an underestimation of the bare Raman cross-sections for some common probes, because of resonance or preresonance conditions, and (iii) the lack of a reliable method to pin down SM events, except for the ultralow concentration approach that led to more uncertainty than answers in many cases.[35] One of the problems of the initially proposed $\sim 10^{14}$ EFs for SM detection is that they are very difficult to justify based on standard electromagnetic theory. This aspect was one of the main arguments in favor of the existence of a chemical contribution to SERS enhancements. The EFs reported here are, in fact, perfectly within our current understanding of electromagnetic SERS enhancements. The comparison of SERS EFs for different analytes further supports the conclusion that chemical contributions to SERS are less common than generally thought. Finally, these results also show that SM-SERS signals occur more often than what is commonly perceived, which was also the conclusion of ref 14.

With the perspective of our ever-evolving understanding of SERS phenomena, we believe that this work presents the most thorough attempt so far to understand the EF properly (both theoretically and experimentally) and to pin down and devise a proper experimental proof for the claims. Our view is that these results are a first step toward bringing to a closure a discussion that showed a spread over several orders of magnitude in the literature for several years.

Acknowledgment. E. C. L. R. and P. G. E. acknowledge financial support from the Royal Society of New Zealand (RSNZ) through a Marsden Grant.

Supporting Information Available: Section S.I gives an overview of the content of the Supporting Information. Section S.II is a lengthy discussion on the different possible definitions of SERS EFs and how they relate to specific situations that are very often found in practice. This section complements Section II of the main paper. Section S.III is an in-depth explanation of the characterization of the non-SERS cross-sections of common SERS probes, including a validation of the cross-sections for reference compounds using Density Functional Theory (DFT) calculations. This section complements the results of Section III, part A, of the main paper. Section S.IV is devoted to a detailed analysis of a very important experimental problem in the determination of SERS cross-sections, namely, the characterization of the exciting beam and detection profile (in short, of the scattering volume) in Raman microscopes. The results of this section are used in Section IV, parts B−D, of the main paper. Section S.V gives additional experimental details on the TDVP experiments, and how the SERS cross-section is extracted from them. It complements Section IV, part D of the main paper. This material is available free of charge via the Internet at http://pubs.acs.org.

References and Notes

(1) Fleischmann, M.; Hendra, P. J.; McQuillan, A. *J. Chem. Phys. Lett.* **1974**, *26*, 163.
(2) Albrecht, M. G.; Creighton, J. A. *J. Am. Chem.* **1977**, *99*, 5215.
(3) Jeanmaire, D. L.; Duyne, R. P. V. *J. Electroanal. Chem.* **1977**, *84*, 1.
(4) Dieringer, J. A.; McFarland, A. D.; Shah, N. C.; Stuart, D. A.; Whitney, A. V.; Yonzon, C. R.; Young, M. A.; Zhang, X.; Duyne, R. P. V. *Faraday Discuss.* **2006**, *132*, 9.
(5) Aroca, R. *Surface Enhanced Vibrational Spectroscopy*; Wiley: Chichester, 2006.
(6) Kneipp, K.; Wang, Y.; Kneipp, H.; Perelman, L. T.; Itzkan, I.; Dasari, R. R.; Feld, M. S. *Phys. Rev. Lett.* **1997**, *78*, 1667.
(7) Nie, S.; Emory, S. R. *Scienc*e **1997**, *275*, 1102.
(8) Kneipp, K.; Kneipp, H. In *Surface-Enhanced Raman Scattering: Physics and Applications*; Kneipp, K., Kneipp, H., Moskovits, M., Eds.; Topics in Applied Physics; Springer: Berlin, 2006; Vol. 103, p 183.
(9) Natan, M. *Faraday Discuss.* **2006**, *132*, 321.
(10) Cai, W. B.; Ren, B.; Li, X. Q.; She, C. X.; Liu, F. M.; Cai, X. W.; Tian, Z. Q. *Surf. Sci.* **1998**, *406*, 9.
(11) Félidj, N.; Aubard, J.; Lévi, G.; Krenn, J. R.; Salerno, M.; Schider, G.; Lamprecht, B.; Leitner, A.; Aussenegg, F. R. *Phys. Rev. B* **2002**, *65*, 075419.
(12) Lal, S.; Grady, N. K.; Goodrich, G. P.; Halas, N. J. *Nano Lett.* **2006**, *6*, 2338.
(13) McFarland, A. D.; Young, M. A.; Dieringer, J. A.; Duyne, R. P. V. *J. Phys. Chem. B* **2005**, *109*, 11279.
(14) Le Ru, E. C.; Meyer, M.; Etchegoin, P. G. *J. Phys. Chem. B* **2006**, *110*, 1944.
(15) Hildebrandt, P.; Stockburger, M. *J. Phys. Chem.* **1984**, *88*, 5935.
(16) Su, K.-H.; Durant, S.; Steele, J. M.; Xiong, Y.; Sun, C.; Zhang, X. *J. Phys. Chem. B* **2006**, *110*, 3964.
(17) Jensen, L.; Schatz, G. C. J. *Phys. Chem. A* **2006**, *110*, 5973.
(18) Graham, D.; McLaughlin, C.; McAnally, G.; Jones, J. C.; White, P. C.; Smith, W. E. *Chem. Comm.* **1998**, *1998*, 1187.
(19) Lee, P.; Meisel, D. *J. Phys. Chem.* **1982**, *86*, 3391.
(20) Meyer, M.; Le Ru, E. C.; Etchegoin, P. G. *J. Phys. Chem. B* **2006**, *110*, 6040.
(21) Le Ru, E. C.; Dalley, M.; Etchegoin, P. G. *Cur. Appl. Phys.* **2006**, *6*, 411.
(22) Le Ru, E. C.; Etchegoin, P. G. *Chem. Phys. Lett.* **2006**, *423*, 63.
(23) Moskovits, M. *J. Chem. Phys.* **1982**, *77*, 4408.
(24) Naumov, S.; Kapoor, S.; Thomas, S.; Venkateswaran, S.; Mukherjee, T. *J. Mol. Structure* (*Theochem*) **2004**, *685*, 127.
(25) Thomas, S.; Venkateswaran, S.; Kapoor, S.; Cunha, R. D.; Mukherjee, T. *Spectrochimica Acta* **2004**, *60*, 25.
(26) Le Ru, E. C.; Etchegoin, P. G.; Meyer, M. *J. Chem. Phys.* **2006**, *125*, 204701.
(27) Kneipp, K.; Wang, Y.; Kneipp, H.; Itzkan, I.; Dasari, R. R.; Feld, M. S. *Phys. Rev. Lett.* **1996**, *76*, 2444.
(28) Brolo, A. G.; Sanderson, A. C.; Smith, A. P. *Phys. Rev. B* **2004**, *69*, 045424.
(29) Haslett, T. L.; Tay, L.; Moskovits, M. *J. Chem. Phys.* **2000**, *113*, 1641.
(30) Le Ru, E. C.; Etchegoin, P. G. *Faraday Discuss.* **2006**, *132*, 63.
(31) Maher, R. C.; Cohen, L. F.; Gallop, J. C.; Le Ru, E. C.; Etchegoin, P. G. *J. Phys. Chem. B* **2006**, *110*, 6797.
(32) Maher, R. C.; Cohen, L. F.; Le Ru, E. C.; Etchegoin, P. G. *Faraday Discuss.* **2006**, *132*, 77.
(33) Maher, R. C.; Cohen, L. F.; Le Ru, E. C.; Etchegoin, P. G. *J. Phys. Chem. B* **2006**, *110*, 19469.
(34) Maher, R. C.; Etchegoin, P. G.; Le Ru, E. C.; Cohen, L. F. *J. Phys. Chem. B* **2006**, *110*, 11757.
(35) Emory, S. R.; Nie, S.; Kneipp, K.; Harrison, G. R. *Chimia* **1999**, *53*, 35.

Supporting information for "SERS enhancement factors: a comprehensive study"

E. C. Le Ru,* E. Blackie, M. Meyer, and P. G. Etchegoin†

The MacDiarmid Institute for Advanced Materials and Nanotechnology
School of Chemical and Physical Sciences
Victoria University of Wellington
PO Box 600, Wellington, New Zealand

S.I. OVERVIEW OF THE SUPPORTING INFORMATION

Herewith we provide all the additional information with full details to complement the results in the main paper.

We start with a lengthy discussion in Sec. S.II on the different possible definitions of SERS EFs and how they relate to specific situations that are very often found in practice. This section is essentially an expanded version of Sec. II of the main paper. Note that some material from Sec. II is repeated here in Sec. S.II to make it entirely self-contained.

We then continue in Sec. S.III with an in-depth explanation of the characterization of the non-SERS cross sections of common SERS probes, including a validation of the cross sections for reference compounds using Density Functional Theory (DFT) calculations. This section complements the results of Sec. III.A of the main paper.

Sec. S.IV is devoted to a detailed analysis of a very important experimental problem in the determination of SERS cross sections, namely, the characterization of the exciting beam and detection profile (in short, of the scattering volume) in Raman microscopes. The latter is an *unavoidable* step to transform measurements on reference compounds into useful values of the SERS cross section in many important situations (in particular for the single molecule SERS problem). The results of this section are used in Secs. IV.B, IV.C, and IV.D of the main paper.

Finally, Sec. S.V gives additional experimental details on the temperature-dependent vibrational pumping experiments, and how the SERS cross-section is extracted from them. It complements Sec. IV.D of the main paper.

S.II. DIFFERENT DEFINITIONS OF THE ENHANCEMENT FACTORS

Here we provide a more lengthy discussion which justifies the different definitions of the enhancement factors provided in the main text. This section should also be viewed as a first attempt toward a rigorous standardization of SERS EFs definitions.

One would ideally like to find a single SERS EF, that is rigorously defined, applies to most situations, can be predicted theoretically, and can be easily measured experimentally. Unfortunately, the complex nature of the SERS effect and SERS substrates makes this impossible. This implies that there are many possible definitions of the SERS EFs, depending on the situation and the effects that are being emphasized. Our approach here is to classify them into three classes:

- The Single Molecule Enhancement Factor (SMEF) and its derivatives.
- The SERS Substrate Enhancement Factor (SSEF) and its derivatives.
- The Analytical Enhancement Factor (AEF) and its derivatives.

We therefore propose a number of rigorous definitions that we consider useful for EFs in each of the three classes, and discuss their respective merits. The accumulation of definitions may appear excessive, but this is unavoidable if rigorous definitions are sought; a necessary step towards the "standardization of SERS". Finally, the respective merits and possible use of these definitions are discussed.

A. General properties of the SERS EFs

In simple terms, the SERS cross section for a given vibrational mode of a given analyte is the normal Raman cross section but affected by an enhancement factor (EF), which may have more than one origin (electromagnetic and/or chemical). By default, we will refer in the following to Stokes Raman scattering, unless otherwise stated. The SERS EFs are usually believed to have two main contributions

- The Electromagnetic Enhancement Factor F_{EM} is thought to be the main contribution. It is due to the coupling of the incident and Raman electromagnetic fields with the SERS substrate and it can usually be separated into two multiplicative EFs, one for the incident field, one for the re-emitted (Raman) field[1].

- Another (multiplicative) contribution to the EF is the so-called chemical enhancement (CE) factor F_{Chem}. Its existence is still subject to controversy[2–5] and its contribution is believed to be much smaller than the EM effect. The CE factor is sometimes viewed as a modification of the electronic polarizability of the probe, which can induce Resonant Raman Scattering (and therefore enhanced signals) at wavelengths where the non-adsorbed molecules would not be resonant[2]. The most widely accepted explanation for this is the Charge Transfer (CT) mechanism[6]. This requires the molecule to be chemically adsorbed on the surface (hence the name chemical enhancement). In this case the CE is essentially a "quantum mechanical effect" resulting in a perturbation of the intrinsic polarizability. It is worth noting however that electromagnetic effects (such as Raman dipole self-reaction)[7–10] could lead to similar results even for physisorbed molecules.

Note that knowing the exact origin of the SERS EFs is, in fact, not necessary when defining them or measuring them experimentally. In the following, we will mostly ignore this origin, therefore encompassing all possible types of enhancements, but still bearing in mind that the EM effect is the dominant one, as shown by an overwhelming majority of experimental evidence.

Moreover, the SERS process (and therefore the enhancement factor) depends on a long list of parameters, including:

- Characteristics of laser excitation, in particular: wavelength, polarization, angle of incidence (for a planar substrate), etc...
- Detection setup, in particular: scattering configuration (e.g. backscattering geometry), solid angle for collection, polarized and/or unpolarized detection, etc...
- SERS substrate, in particular: material (usually silver or gold), geometry, orientation with respect to incident beam direction and polarization. The dimensionality of the substrate (e.g. 2D planar substrate or 3D colloidal solution) is also an important parameter since it requires different sample preparation procedures.
- Intrinsic properties of the analyte, in particular: Raman tensors of the modes and intrinsic Raman cross-sections.
- SERS analyte adsorption properties, in particular: adsorption efficiency (surface coverage), distance from the surface[2,11], adsorption orientation (fixed or fluctuating), and modification of Raman polarizability induced by adsorption. This latter aspect is essentially the chemical contribution to SERS while, the previous one provides the background and origin of surface selection rules[12].

It is difficult to account for all of these parameters and many of them may, in fact, be unknown. In defining a SERS EF, the aim is to find a definition that: (*i*) is independent of as many parameters as possible (or at least gives a good estimate for a wide range of parameters), (*ii*) can be either easily measured experimentally or predicted theoretically (and ideally both), and (*iii*) allows for a direct comparison of the merits of different SERS substrates. It is impossible to meet all these criteria, since an accurate SERS EF taking into accounts all possible parameters is necessarily complex and suited only to very specific and limited conditions. Contrariwise, a simple definition of the SERS EF that would apply to most situations can only be approximate, since it does not take into account, say, the Raman tensors or chemical properties of the probe.

With these considerations in mind, we will consider in the following several possible definitions of the SERS EF and discuss their merits and problems. The definitions will start accumulating once the different scenarios are contemplated and, for clarity, they have been summarized in Table S.I. We will also ignore in the following definitions the possible complications associated with photobleaching or photo-desorption of the analytes. These effects can strongly affect any experimental measurements but can (and should) be avoided by a careful choice of the probe and/or power density for excitation.

B. The single molecule enhancement factor

SERS enhancements on most SERS substrates are highly non-uniform, especially on the molecular scale of nanometers. Points of high enhancements, "hot-spots", are generally highly localized, and can be within tens of nanometers of points with no enhancements at all. Most SERS EFs reported in the literature correspond to *spatially-averaged EFs*, and ignore this non-uniformity. However, for some applications, in particular in relation to single molecule SERS (SM-SERS), the most relevant quantity is the enhancement at some specific positions, usually the "hot-spots". To account for this, it is therefore useful to define the *Single Molecule Enhancement Factor* (SMEF). This is the SERS enhancement felt by a given molecule at a specific point. It is in general dependent on the Raman tensor of the probe and its orientation on the SERS substrate and with respect to the local field at that point. It is also dependent on the orientation of the SERS substrate with respect to the incident laser polarization and direction. Hence, it requires the exact definition of the SERS substrate geometry, and the exact position and orientation of the probe on it. Because of these constraints, this definition is much more suited to theoretical estimations of the EF, rather than experimental measurements.

The SMEF could be defined simply as the ratio of the SERS intensity of a single molecule $I_{\text{SERS}}^{\text{SM}}$ to the Raman intensity $I_{\text{RS}}^{\text{SM}}$ of the same molecule under the exact same

conditions, but in the absence of the metallic SERS substrate. However, the definition as stated above presents a major shortcoming because the SERS intensity is compared to that of the free molecule in a fixed position and orientation. This means that, even if the SERS intensity was identical for different positions and orientations of the probe, the SMEF could vary because of different Raman signals from the free molecule. To illustrate this problem, one can consider the extreme case of a highly uniaxial Raman tensor with axis perpendicular to the exciting polarization. The Raman intensity of the free molecule would then be zero, while the SERS intensity could be finite (possibly small) since the SERS substrate can modify the local field polarization. This would result in an infinite EF, which would certainly not reflect the overall magnitude of the SERS signal. To avoid this problem, we therefore suggest the following definition for the Single Molecule Enhancement Factor given in the main paper:

$$\mathrm{SMEF} = \frac{I_{\mathrm{SERS}}^{\mathrm{SM}}}{\langle I_{\mathrm{RS}}^{\mathrm{SM}} \rangle}, \tag{S1}$$

where $I_{\mathrm{SERS}}^{\mathrm{SM}}$ is the SERS intensity of the single molecule under consideration, while $\langle I_{\mathrm{RS}}^{\mathrm{SM}} \rangle$ is the *average* Raman intensity per molecule for the same probe, also discussed in Sec. III.B. This average is to be taken over all possible (random) orientations of the molecule in space. Hence, this average only depends on the Raman tensor of the probe, and is independent of the molecule position or orientation. It can be estimated experimentally by measuring the Raman intensity of, for example, a solution of known concentration. It is worth noting that $\langle I_{\mathrm{RS}}^{\mathrm{SM}} \rangle$ may depend on the solvent because of possible interactions with the solvent molecules. It also depends on the refractive index of the solvent because of the local field corrections (see Sec. S.III.D). For a rigorous definition, we will therefore impose as a convention that $\langle I_{\mathrm{RS}}^{\mathrm{SM}} \rangle$ is measured in water (whenever possible) or a solvent of similar refractive index.

C. Link to SERS cross-sections

One advantage of the definition of the previous subsection is that it can be simply expressed in terms of cross-sections. Note that in defining a SERS cross-section we encounter some of the same problems as when defining the SMEF: it depends for example on the substrate and its orientation, on the molecule position and its orientation with respect to the surface (which can be averaged or not), etc... One cannot therefore define a single SERS cross-section, as is the case for normal Raman processes. For a given set of parameters (which need to be clearly stated) one can however define a *differential SERS cross-section* in a similar way as for the non-SERS case:

$$I_{\mathrm{SERS}}^{\mathrm{SM}} = \frac{d\sigma_{\mathrm{SERS}}}{d\Omega}\, S_0 \delta\Omega, \tag{S2}$$

where S_0 is the incident laser intensity, $\delta\Omega$ the solid angle for collection, and $I_{\mathrm{SERS}}^{\mathrm{SM}}$ is the SERS intensity of a given single molecule (note that there is no orientation averaging here since the adsorption geometry may be fixed). This definition allows us, for example, to compare $d\sigma_{\mathrm{SERS}}/d\Omega$ to the differential cross-section of other processes such as fluorescence. It also allows us to write the SMEF defined in Eq. S1 as a ratio of SERS over non-SERS differential cross-sections:

$$\mathrm{SMEF} = \frac{d\sigma_{\mathrm{SERS}}}{d\Omega} \Big/ \frac{d\sigma_{\mathrm{RS}}}{d\Omega}. \tag{S3}$$

Although it is not directly related to SERS EFs it is worth digressing here to discuss other possible types of SERS cross-sections. By integrating the differential SERS cross-section over all detection directions, it is possible to define the *integrated radiative SERS cross-section* σ_{SERS}. As for the non-SERS case, this quantity is difficult to measure (it requires an integrating sphere, for example). Moreover, it is in general not as straightforward as in the non-SERS case to derive it from the differential cross-section. There is an additional peculiarity to the SERS case: because the metallic SERS substrate is optically absorbing, some of the SERS scattered photons are absorbed and cannot be detected in the far-field. They correspond to non-radiative SERS processes, where the SERS process does occur in the molecule (excitation of a vibration), but the Stokes-scattered photon is re-absorbed in the metal. The radiative SERS cross-section σ_{SERS} does not include such processes and is therefore not an exact representation of what is actually felt by the molecule (in terms of the number of vibrations created). We can therefore define a *total SERS cross-section* σ_{Tot}, which includes both radiative events (in all directions) and non-radiative ones. One could argue that this subtlety is irrelevant since it is usually non-observable. There is however at least one situation where this cross-section is measured: in SERS vibrational pumping experiments.[13,14] We will come back to this point in Sec. S.V.

D. Orientational effects

For a given probe, the proposed definition of the SMEF directly reflects the SERS intensity for a given molecule position/orientation on a SERS substrate. However, the molecule orientation is not necessarily known or even fixed during the time of a measurement. It can therefore also be useful to define the Orientation-Averaged SMEF (OASMEF) at a given position as:

$$\mathrm{OASMEF} = [\mathrm{SMEF}] = \frac{\left[I_{\mathrm{SERS}}^{\mathrm{SM}}\right]}{\langle I_{\mathrm{RS}}^{\mathrm{SM}} \rangle}, \tag{S4}$$

where the average denoted by $[\ldots]$ is to be taken over all *allowed* orientations of the molecule in SERS conditions (not to be confused with the real orientation averaging

denoted $\langle \ldots \rangle$). There are situations where this average is not necessary. For example, for an isotropic Raman tensor, OASMEF and SMEF are identical since the SMEF depends only on the position of the probe, not on its orientation. However, for a highly uniaxial tensor, the SMEF now depends on $\mathbf{e}_d$: the orientation of the axis. If the molecule is known to adsorb with its axis perpendicular to the metallic surface, then $\mathbf{e}_d$ is well defined and equal to the local normal unit vector $\mathbf{n}$, and again no averaging is needed. But, if the molecule adsorbs with its axis tangential to the metallic surface, then there remains one degree of rotational freedom; the axis is not well defined and averaging is needed over one angle (rotation in the tangential plane). Similarly, if adsorption can occur in any possible orientation, then averaging is needed over two angles representing all possible orientations in space. Like most SERS EFs, the SMEF and OASMEF depend on the excitation wavelength and mode energy (Raman shift), and also on the symmetry of the Raman tensor of the mode.

The SMEF or OASMEF provide a measure of the SERS EF for a given SERS substrate at a given position, for example a "hot-spot". Using these definitions, SERS enhancements can then be easily compared for different positions on a SERS substrate, and maximum EFs between two different SERS substrates, at least at a theoretical level. Moreover, when no chemical enhancements are involved the SMEF should be the same for all probes with the same Raman tensor symmetry. This definition of the SMEF is therefore, in our opinion, the most unbiased estimation of the SERS enhancements for a single molecule. It should be calculated or measured with probes ideally showing no chemical enhancements, and with representative Raman tensors, such as isotropic, planar isotropic, or highly uniaxial tensors.

Finally we note that in most cases, what is important is the maximum SMEF on a SERS substrate. This is particularly true for experiments, where single molecule signals may only be detectable from the points of highest enhancements (hot-spots).

E. The SERS substrate point of view

For many SERS applications and experiments, the detailed distribution of the SMEF on the substrate, or even its maximum value, is irrelevant since one is mainly dealing with average SERS signals. It is therefore equally important to define one or more SERS Substrate Enhancement Factors, which can be used to compare the average SERS enhancements across different substrates. In fact, most studies of SERS EFs so far have indeed focused on this aspect. The most widely used definition for the average SERS EF is:[15–19]

$$\mathrm{EF} = \frac{I_{\mathrm{SERS}}/N_{\mathrm{Surf}}}{I_{\mathrm{RS}}/N_{\mathrm{Vol}}}, \tag{S5}$$

where $N_{\mathrm{Vol}} = c_{\mathrm{RS}}V$ is the average number of molecules in the scattering volume (V) for the Raman (non SERS) measurement, and N_{Surf} is the average number of *adsorbed* molecules in the scattering volume for the SERS experiments. This definitions presents a few problems:

- It first requires additional constraints to make it more rigorous, in particular in terms of which molecules exactly should be counted in N_{Surf}. For example, a natural question one can ask for a 2D planar SERS substrate is whether we should count only the molecules adsorbed on the metal, or also those adsorbed on non-metallic parts in between. The same question applies to molecules in the first layer as opposed to those in subsequent layers. Quite clearly, the fact that a given concentration is put on the sample does not mean that this concentration is the relevant one to produce the measured SERS signal.

- Secondly, the notion of scattering volume is not rigorous in many cases and the exact metallic surface area is not easily measured (in samples with complicated topology, for example); the final EF will depend on how these are estimated. Strongly related to this problem is the fact that the excitation intensity, even the most ideal of situations, is usually not uniform across the scattering volume.

Because of these issues, the definition above is not rigorous enough and could lead to artificial variations by as much as 2 orders of magnitude for the measured EF on a given substrate.

In an attempt to remedy to these problems, we will formally define the *SERS substrate Enhancement Factor* (SSEF), directly from the SMEF, and then show how this formal definition relates to the commonly used expression above. Recall that the SMEF can be defined at every point $\mathbf{r}$ on the surface of the substrate. The OASMEF is then simply deduced by orientation-averaging over allowed orientations as discussed previously. The SSEF can then be defined formally as:

$$\mathrm{SSEF} = \frac{1}{A_M}\int_{A_M} \mathrm{OASMEF}(\mathbf{r})\; dS, \tag{S6}$$

where A_M represents the surface area of the metallic substrate. This last expression can be rewritten as:

$$\mathrm{SSEF} = \{\mathrm{OASMEF}\} = \{[\mathrm{SMEF}]\}, \tag{S7}$$

where $\{[\mathrm{SMEF}]\}$ is the spatial-and-allowed-orientation-averaged single molecule EF, and it is the expression given in the text.

The above definition is strictly rigorous and well suited to theoretical predictions, but it is now necessary to relate it to experimental measurements and to the commonly used expression given in Eq. S5. Because this expression has mostly been used in the past for 2D planar SERS substrate, we will focus in the following on this particular case. This is also the most difficult case because of

Name	Acronym	Definition	Depends on
Enhancement Factor	EF	-	-
Electromagnetic EF	F_{EM}	-	-
Chemical EF	F_{Chem}	-	-
Analytical EF	AEF	$(I_{\mathrm{SERS}}/c_{\mathrm{SERS}})\,/\,(I_{\mathrm{RS}}/c_{\mathrm{RS}})$ (Eq. S13)	λ_L, $\bar{\nu}_i$, $\underline{\tilde{\alpha}}$, $\mathbf{e}_m$, IP
SERS Substrate EF	SSEF	(Eqs. S6,S7,S12)	λ_L, $\bar{\nu}_i$, $\underline{\tilde{\alpha}}$, $\mathbf{e}_m$, IP
Total SERS Substrate EF	TSSEF	SSEF$\times$ metal surface coverage	λ_L, $\bar{\nu}_i$, $\underline{\tilde{\alpha}}$, $\mathbf{e}_m$, IP
Polarization Averaged SSEF	PASSEF	Obtained by averaging SSEF over polarizations	λ_L, $\bar{\nu}_i$, $\underline{\tilde{\alpha}}$, $\mathbf{e}_m$
Single Molecule EF	SMEF	$I^{\mathrm{SM}}_{\mathrm{SERS}}/\langle I^{\mathrm{SM}}_{\mathrm{RS}}\rangle$ (Eqs. S1,S3)	λ_L, $\bar{\nu}_i$, $\underline{\tilde{\alpha}}$, $\mathbf{e}_m$, IP
Orientation Averaged SMEF	OASMEF	$\left[I^{\mathrm{SM}}_{\mathrm{SERS}}\right]/\langle I^{\mathrm{SM}}_{\mathrm{RS}}\rangle$ (Eq. S4)	λ_L, $\bar{\nu}_i$, $\underline{\tilde{\alpha}}$, IP
Electromagnetic SSEF	EMSSEF	SSEF for purely EM enhancement	λ_L, $\bar{\nu}_i$, $\underline{\tilde{\alpha}}$, $\mathbf{e}_m$, IP
Electromagnetic SMEF	EMSMEF	SMEF for purely EM enhancement	λ_L, $\bar{\nu}_i$, $\underline{\tilde{\alpha}}$, $\mathbf{e}_m$, IP
Isotropic (tensor) EMSSEF	Iso-EMSSEF	EMSSEF for an isotropic Raman mode	λ_L, $\bar{\nu}_i$, IP
Isotropic (tensor) EMSMEF	Iso-EMSMEF	EMSMEF for an isotropic Raman mode	λ_L, $\bar{\nu}_i$, IP
Differential Raman cross section	$d\sigma_{\mathrm{RS}}/d\Omega$	see Secs. S.III.B and S.III.C	λ_L, $\bar{\nu}_i$, α_0
Differential SERS cross section	$d\sigma_{\mathrm{SERS}}/d\Omega$	see Sec. S.II C, Eq. S2	λ_L, $\bar{\nu}_i$, $\underline{\tilde{\alpha}}$, α_0, $\mathbf{e}_m$, IP
Integrated radiative SERS cross section	σ_{SERS}	see Sec. S.II C	λ_L, $\bar{\nu}_i$, $\underline{\tilde{\alpha}}$, α_0, $\mathbf{e}_m$, IP
Total SERS cross section	σ_{Tot}	see Sec. S.II C	λ_L, $\bar{\nu}_i$, $\underline{\tilde{\alpha}}$, α_0, $\mathbf{e}_m$, IP

TABLE S.I: Summary of acronyms, notations, and definitions. The dependence of some of these enhancement factors upon the following parameters is also specified: Excitation wavelength (λ_L), mode vibrational energy or wavenumber $\bar{\nu}_i$, type or symmetry of the Raman tensor $\underline{\tilde{\alpha}}$, molecular adsorption geometry $\mathbf{e}_m$, substrate orientation with respect to incident polarization (IP) when not averaged.

the problems of comparing signals originating from a 2D structure to that of a 3D volume. Let us consider a SERS experiment on such a substrate consisting of a repeating pattern of individual sub-wavelength metallic structures (which is representative of many practical cases). Let μ_M [m^{-2}] be the surface density of the individual nanostructures with respect to the main plane forming the substrate, and A_M is the metallic surface area in each structure (usually larger than the projected surface area or shadow of the structure on the main plane). The excitation is usually non-uniform and characterized in the focal plane by an intensity profile $S(\rho)$ [$\mathrm{W\,m}^{-2}$] and a corresponding power P [W], which can be obtained by integration of $S(\rho)$. We assume the excitation area is much larger than the individual structures forming the substrate and that the exciting intensity is approximately uniform for a given single structure. From the definitions of the previous section, one molecule at a given position $\mathbf{r}'$ on the surface of an individual metallic object at a position ρ within the beam, emits a SERS signal equal to

$$I(\mathbf{r}') = \mathrm{OASMEF}(\mathbf{r}')\frac{d\sigma_{\mathrm{RS}}}{d\Omega}S(\rho)\delta\Omega \tag{S8}$$

Assuming a surface density of molecules μ_S [m^{-2}] on the metal, the SERS signal for this single structure is then

$$I^{\mathrm{Single}}_{\mathrm{SERS}} = \mu_S A_M\{\mathrm{OASMEF}\}\frac{d\sigma_{\mathrm{RS}}}{d\Omega}S(\rho)\delta\Omega \tag{S9}$$

Integrating now over all the metallic objects in the beam, we obtain the total SERS signal:

$$I_{\mathrm{SERS}} = \mu_M\mu_S A_M\{\mathrm{OASMEF}\}\frac{d\sigma_{\mathrm{RS}}}{d\Omega}P\delta\Omega \tag{S10}$$

We now compare this SERS signal to that obtained in non-SERS conditions (I_{RS}) from a solution of concentration c_{RS}. We must relate I_{RS} to $d\sigma_{\mathrm{RS}}/d\Omega$ and P. The non-uniform excitation is here again a problem, and it is made more complicated here because of the 3D nature of the scattering volume. In fact, the collection efficiency is not uniform along the beam axis and depends on the experimental setup (confocal depth). The same issue arises when estimating experimentally the SMEF and it is therefore discussed in detail Sec. S.IV, from where we borrow here the result:

$$I_{\mathrm{RS}} = c_{\mathrm{RS}}H_{\mathrm{eff}}\frac{d\sigma_{\mathrm{RS}}}{d\Omega}P\delta\Omega, \tag{S11}$$

where H_{eff} is defined in in Sec. S.IV and is the effective height of the scattering volume.

Our formal definition of the SSEF can now be expressed in terms of the experimentally measured signals as

$$\mathrm{SSEF} = \frac{I_{\mathrm{SERS}}/(\mu_M\mu_S A_M)}{I_{\mathrm{RS}}/(c_{\mathrm{RS}}H_{\mathrm{eff}})} \tag{S12}$$

This expression reduces to Eq. S5 when defining $N_{\mathrm{Surf}} = \mu_M\mu_S A_M A_{\mathrm{eff}}$, and $N_{\mathrm{Vol}} = c_{\mathrm{RS}}V = c_{\mathrm{RS}}H_{\mathrm{eff}}A_{\mathrm{eff}}$. A_{eff} is the effective surface area of the scattering volume (the equivalent of a scattering volume but for 2D). This rigorous derivation highlights a number of important aspects for the experimental determination of the SSEF:

- The parameter A_{eff} has been introduced to express Eq. S12 in terms of N_{Surf} and N_{Vol} but is in fact irrelevant to the final result. The only relevant aspect of the scattering volume is the effective height,

which needs to be characterized carefully (as we shall show later in Sec. S.IV). This length scale here enables the connection between 2D and 3D measurements.

- In our derivation, we have considered only molecules directly adsorbed on the metal surface. In experiments, it is important that the surface coverage remains smaller than (or equal to) one monolayer when using Eq. (S5) or (S12). This is because the SERS effect is distance-dependent and the SERS signal from molecules on the second monolayer is usually reduced.[2,11] This additional constraint ensures that the average SERS intensity is proportional to the average number of adsorbed molecules, which is necessary for Eq. (S5) and (S12) to represent a physically meaningful quantity.

Finally, in the previous definitions N_{Surf} corresponds to the number of molecules adsorbed *on the metallic surface*. This choice emphasizes the EF of each individual structure (for periodic patterns), as opposed to that of the entire substrate as a whole. If alternatively, the total number of molecules (i.e. those adsorbed on the metal plus those adsorbed elsewhere on the surface in between the metallic structures) is chosen, then a smaller EF is obtained and we call it the *Total SERS Substrate EF* (TSSEF). The TSSEF is then simply the SSEF times the percentage surface coverage of the metal. The distinction between SSEF and TSSEF has already been emphasized[15] and can be important when comparing EFs. The proportion of the total surface that is occupied by the metal can be as low as 7%[16], which result in a factor of ≈ 15 between SSEF and TSSEF. The SSEF is more relevant in situations where the analyte selectively attaches on the metal only, but the TSSEF is more important if adsorption is not selective.

Once a rigorous definition such as those above is agreed, comparison between SERS substrates is in principle possible, but there can still be many discrepancies in the measured SSEF or TSSEF because of experimental problems, in particular:

- It is not always easy to ensure that one (or less) monolayer is adsorbed. In general, it is assumed to that exactly one monolayer is adsorbed based on chemical arguments (such as covalent bonding of the first layer, followed by rinsing of subsequent layers), but no independent confirmation is sought. Alternatively, it is sometimes argued that only the first layer gives rise to SERS, thereby eliminating the problem associated with subsequent layers. However, recent results[2,11] have shown that the distance dependence of the SERS effect is not in general as dramatic as originally sought and the first layer argument may then be wrong, at least in some situations. Adsorption isotherm studies[20] can remedy some of these uncertainties, but are not always feasible.
- Even if one monolayer is adsorbed, an accurate estimation of the molecule surface density ρ_S is in most cases difficult, which results in uncertainties in the derived SSEFs.
- Other uncertainties can be associated with the value of H_{eff} if the scattering volume is not carefully characterized.

We believe that the rigorous definition and careful derivation of the SSEF given above is a first step towards reducing uncertainties and "standardizing" SSEF measurements. However, until new tools are developed to address some of the issues mentioned above, the comparison of SSEFs among substrates remains problematic.

Finally, note that we have implicitly assumed here a pre-determined geometry for the SERS substrate, fixed with respect to the incident field polarization. In some cases (for example in colloidal solutions) we do not have such control on the orientation of the substrate with respect to the incident polarization. We can therefore define a polarization-averaged SSEF as PASSEF $= \langle \mathrm{SSEF} \rangle$ where $\langle \ldots \rangle$ means the average over all possible orientation of the substrate with respect to the incident polarization. The SSEF (or PASSEF) remains dependent on the excitation wavelength and mode energy (Raman shift), and also on the symmetry of the Raman tensor of the mode under consideration.

F. The analytical chemistry point of view

The definitions introduced so far, SMEF and SSEF, have attempted to emphasize the intrinsic characteristics of the substrate and are not always straightforward to relate to experimental results. For many applications, however, one is mostly concerned with the simple question of how much more signal can be expected from SERS as compared to normal Raman under given experimental conditions. To address this question, we introduce another definition of the SERS EF, which is fairly intuitive and particularly relevant for analytical chemistry applications. Let us consider an analyte solution with concentration c_{RS}, which produces a Raman signal I_{RS} under non-SERS conditions. Under identical experimental conditions (laser wavelength, laser power, microscope objective or lenses, spectrometer, etc), and for the same preparation conditions, the same analyte on a SERS substrate, with possibly different concentration c_{SERS}, now gives a SERS signal I_{SERS}. The *Analytical Enhancement Factor* (AEF) can then be defined as:

$$\mathrm{AEF} = \frac{I_{\mathrm{SERS}}/c_{\mathrm{SERS}}}{I_{\mathrm{RS}}/c_{\mathrm{RS}}}. \tag{S13}$$

This definition, although useful for specific practical applications, tends to depend strongly on many factors, in particular on the adsorption properties and surface coverage (monolayer vs. multilayer) of the probe; in

fact c_{SERS} does not characterize well the number of adsorbed molecules. It is also strongly dependent on the sample preparation procedure for 2D planar substrates (e.g. spin-coating, dipping, or drying). The AEF in fact ignores the fact that SERS is a type of *surface spectroscopy*, which means that only the adsorbed molecules contribute to the signal, and that the effect is distance-dependent.[2,11] For this reason, it is not a good characterization of the SERS substrate itself, and cannot be used to easily compare the performances of different substrates. However, provided all experimental procedures are clearly stated, the AEF represents a simple figure for the SERS EF, whose measurement is easily reproducible. From its definition, is is also clear that the AEF is particularly suited to the case of SERS active liquids, e.g colloidal solutions.

It is possible, at least in theory, to relate the AEF to the SSEF, but this step is more case-specific. One needs to take into account the possible effects of adsorption efficiency of the analyte, number of layers of analytes on the substrate if more than one monolayer (distance dependence), orientation of the substrate with respect to incident polarization, polydispersity of the SERS substrate (e.g. for colloids), preparation conditions, etc. Let us consider for example the case of solutions containing colloidal aggregates and let us assume sub-monolayer coverage and total adsorption of the analyte for simplicity, a case relevant to the experiments presented in Sec. III.C of the main paper. Even if the SSEF of a particular aggregate is known, one first needs to average over possible orientations of the aggregate in solution (PASSEF). This would correspond to the actual AEF only if all aggregates were exactly identical. This is unrealistic in practice, where aggregates differ in particular in their resonance condition with the laser (and therefore in the magnitude of their PASSEF). An averaging of the PASSEF over all types of aggregates is then required to obtain the AEF.

Another example of interest is the case of planar SERS substrates. Well-defined structures can now be fabricated using nano-lithography techniques.[11,15,16] The SSEF can therefore be in principle calculated. The AEF could then be predicted for a specific probe, but will depend on the preparation conditions, i.e. how the analyte is transferred from solution to the substrate (dipping, drying, spin-coating, etc...).

G. Merits of the different definitions

We now discuss and compare the merits of the previous definitions of the SERS EFs.

The AEF is the easiest to measure experimentally, and is directly relevant to many applications. It does provide a meaningful and easy-to-interpret figure for the EFs when conditions are clearly defined, but this figure may change easily with exact experimental conditions (even with analyte concentration for example). It is, moreover, difficult to model theoretically. For these reasons, it is not an appropriate definition to characterize rigorously and compare SERS substrates. The definitions of SSEF and SMEF are much more suited to this end. They characterize two important aspects of a SERS substrate: its average and maximum SERS EF, respectively.

These definitions can be used in two ways: The first is to choose a specific analyte/metal combination, along with a set of parameters (polarization, wavelengths, etc). The SSEF and SMEF are then very specific to this situation, but can be used to compare the characteristics of SERS substrates with, say, different geometries. Despite this, they cannot be used as a general characterization of the merits of the substrate because they are too specific (to the metal/analyte combination in particular). If the analyte for example exhibits a large chemical enhancement, the SSEF or SMEF would be larger for this analyte than for some others. It is therefore not an intrinsic property of the substrate.

The second approach seeks to find such an intrinsic EF, and this can be achieved by taking the following steps:

- To properly characterize a SERS substrate, the SMEF (and SSEF) should be independent of the chosen analyte. The first pre-requisite for this is to measure it using a molecule for which there is no chemical enhancement. The absence of CE can sometimes be guessed but is not always easy to prove experimentally. The best approach to resolve this experimentally is therefore to measure the SMEF (SSEF) with different analytes. If the same value is obtained, it is a strong indication that the SMEF (SSEF) is meaningful and that the chosen analytes do not experience any appreciable CE (otherwise its magnitude would be the same, an unlikely coincidence for different molecules). The obtained value is then the *electromagnetic SMEF* (EMSMEF), or *electromagnetic SSEF* (EMSSEF), which are then mostly independent of the analyte.

- The Raman tensor of the mode and molecule orientation can still influence slightly the value of the EMSMEF because of surface selection rules.[12] One simple convention is to consider the EMSMEF for fully isotropic modes, which we will call Iso-EMSMEF (and the corresponding Iso-EMSSEF). This makes theoretical calculations easier but is not always practical experimentally. However, if the EMSMEF is measured for a mode where the Raman tensor and orientation are known, it is then possible to deduce the Iso-EMSMEF from simple theoretical arguments.

- Finally, the Iso-EMSSEF and Iso-EMSMEF remain dependent on a (smaller) number of parameters, which therefore needs to be clearly stated when quoting or comparing values. They are dependent on the excitation wavelength and, to a lesser degree, on the vibrational mode energy (Stokes energy), and possibly incident polarization. With this

in mind, this two SERS EFs are in our opinion the most general and rigorous definitions to compare the merits of various SERS substrates in terms of average and single molecule enhancement.

Before this section, we critically analyze the list of definitions introduced in this Section and their possible use

- There are three classes of SERS EFs: each represented by the SMEF, the SSEF, and the AEF. These three EFs were defined from an experimental perspective and are therefore well suited to measurements (although not without some difficulties).
- Some of their derivatives we introduced such as the *orientation averaged single molecule EF* (OASMEF), the *total SERS substrate EF* (TSSEF), or the *polarization averaged SERS substrate EF* (PASSEF), were introduced mainly to accommodate other common experimental situations, in an attempt to be exhaustive.
- These EFs (quoted above) can all be measured rigorously using the definitions provided in this Section. However, they depend on a number of parameters, and in particular the SERS probe. They therefore do not provide as such a good figure of merit to compare the performances of a given substrate.
- To this end, one should use the Iso-EMSMEF and Iso-EMSSEF. These can in principle be measured from experiments on one or more adequate SERS probes. They can also in principle be easily predicted theoretically.

This list of rigorous definitions should provide a good basis on which various SERS EFs measurements can be compared. They also prove the point of how difficult it is to find general definitions that would work in all possible situations. The classification provided here, however, is a first step to remove one possible artificial source of variability in the SERS EF quoted in the literature which comes simply due to different definitions. There remain many problems associated with the assumptions that are made when estimating a given SERS EFs from a given SERS measurements; for example, how to estimate surface coverage, how to ensure the single molecule nature of a SERS signal, etc... These assumptions must be clearly stated and explained to enable others to analyze critically the validity of the SERS EF. The definitions also clearly highlight the need to characterize first the non-SERS properties of the molecule under considerations. We will show later, for example, that some of the misconceptions found in the literature (like the claim of an enhancement factor of 10^{14} needed to see single molecules) come, in part, from an improper definition and normaliztion of the enhancement factors. Table S.I provides a summary of all the definitions introduced here and in the main companion paper.

S.III. THE DETERMINATION OF NON-SERS CROSS SECTIONS

We discuss in this section all the information that is required to characterize the normal (non-SERS) cross section of typical SERS probes. The determination of "non-SERS" Raman cross sections is neither needed for countless other applications of SERS nor is it a new subject in Raman spectroscopy. Nonetheless, the main problem (as far as the determination of enhancement factors in SERS is concerned) is that the required information is typically spread out over tens of references and books, some of which might not be widely available. An example of the latter is Ref. 21, which is a comprehensive review of the basic aspects of Raman cross section determination and contains an important list of early results for absolute cross sections of relevant standard liquids and gases. For the determination of the SERS enhancement factor, the "bare" Raman signal of the probe is an important normalization factor and this step cannot be avoided. The results of this Section cover accordingly some "textbook-like" material, which we apply to specific examples relevant to SERS enhancement factors.

Although a *relative* measurement of the Raman (non-SERS) cross-section is usually sufficient to determine SERS EFs, knowing the *absolute* Raman cross-section is of great interest for several reasons: (*i*) it highlights the fact that many SERS probes are in fact already very good Raman (non-SERS) scatterers; (*ii*) it is necessary if one wishes to determine the absolute SERS cross section from the SERS EF (for example, in order to be able to compare the effect with fluorescence); and (*iii*) in temperature-dependent vibrational pumping experiments,[13,14] where the absolute SERS cross section is measured, the absolute Raman cross-section is required to determine the SERS EF. Consequently, the objectives of this Section can be summarized as follows: (*i*) to collect and standardize the definitions of the bare Raman cross section (this is sometimes the source of confusion, in particular in relation to the pre-factors of the scattering cross section and the connection between the Raman polarizability and the Raman tensor), (*ii*) to provide and summarize data for a standard compound that can be used as a "calibration" or reference compound by other researchers, and (*iii*) to provide measurements of the absolute Raman cross-section of a set of representative SERS probes. Last, but not least, we show the utility of Density Functional Theory (DFT) calculations for the obtention of absolute Raman cross sections. DFT is a tool that is slowly becoming of widespread use with modest computational resources. It has mostly been used so far to predict the vibrational

mode energies, and assign them to their respective normal modes. We demonstrate here its predictive power for the absolute Raman cross-section of simple non-resonant compounds, thus providing an additional layer of confidence in the overall consistency of the calculated and measured values for the cross sections.

A. Definitions and calculations of Raman cross-sections

The rigorous definition of the Raman cross-sections and, for example, the distinction between total and differential cross-sections, is one of the most basic aspects of Raman spectroscopy. These issues have, however, seldom been discussed in a SERS context. In order to first set the notations and assemble the most important definitions, we here briefly review the main ingredients of the theory of Raman intensities and tensors.[21–23] Units are quoted in between brackets [...] for added clarity. S.I. units (or their derivatives) are used unless otherwise stated and ϵ_0 [$\mathrm{m^{-3}\,kg^{-1}\,s^4\,A^2}$] (permittivity of vacuum) may be used as a "unit" to simplify some expressions.

B. Definitions of Raman cross-sections

We consider a Raman measurement on a molecule (or a collection of identical molecules) in a liquid or gas state, and denote $\langle I_{\mathrm{RS}}^{\mathrm{SM}}\rangle$ [W] the Raman scattered intensity of a given vibrational mode by a single molecule, averaged over all random orientations of the molecule in space. By definition, it is related to the *absolute differential Raman cross-section* $d\sigma_{\mathrm{RS}}/d\Omega$ [$\mathrm{m^2\ sr^{-1}}$] of the vibrational mode via:

$$\langle I_{\mathrm{RS}}^{\mathrm{SM}}\rangle = \frac{d\sigma_{\mathrm{RS}}}{d\Omega} S_0 \delta\Omega, \quad \text{where} \quad S_0 = \frac{\epsilon_0 c}{2}\sqrt{\epsilon_M}|E_0|^2 \tag{S14}$$

is the incident laser intensity [$\mathrm{W/m^2}$] at the molecule position in a medium of dielectric constant ϵ_M and $\delta\Omega$ [sr] is the small solid angle for light collection. Note that *by definition*:[21,24] (i) the absolute differential Raman cross-section is an orientation-averaged property, and (ii) the above expression is strictly valid only for either back-scattering, forward scattering, or 90° scattering geometries.

Another important characteristic of a Raman mode is its depolarization ratio,[21,24] ρ (ratio between the average Raman intensities for polarized detection perpendicular and parallel, respectively, to the incident polarization). In standard Raman spectroscopy, ρ only depends on the symmetry (or more precisely on the symmetry of the Raman tensor) of the mode under consideration.

The differential cross-section corresponds to the Raman signal that can be measured in a given detection direction, but in reality, Raman photons are emitted in all directions, with a specific radiation profile (angular dependence). The *total (or integrated) absolute Raman cross-section*, σ_{RS} [$\mathrm{m^2}$] is the total cross-section integrated over all possible detection directions. It is the cross-section of the Raman process, as felt by the molecule, independent of detection. It is in general difficult to measure experimentally since one would, for example, need to use an integrating sphere. It can alternatively be derived from the absolute differential Raman cross-section through the expression:[21]

$$\sigma_{\mathrm{RS}} = \frac{8\pi}{3}\frac{1+2\rho}{1+\rho}\,\frac{d\sigma_{\mathrm{RS}}}{d\Omega}. \tag{S15}$$

σ_{RS} is typically larger than $d\sigma_{\mathrm{RS}}/d\Omega$ by a factor of ~ 10 for typical collection geometries.

When quoting absolute Raman cross-sections, it is very important to clearly define which cross-section, integrated or differential, is considered. The distinction between these two cross-sections has sometimes been overlooked in the estimation of SERS EFs, which automatically results in errors of an order of magnitude.

C. Semi-classical approach to Raman cross-sections

The semi-classical approach to Raman scattering[22] is important here for several reasons. As we will show in the following, it can be used to predict successfully the absolute non-SERS cross-sections of small non-resonant molecules. Moreover, for larger more resonant molecules for which this approach fails to predict the Raman intensities or the Raman polarizability tensor, the Raman polarizability can still be taken as an input parameter within the semi-classical approach and used to predict SERS cross-sections or enhancements.

The differential Stokes cross-section of a given vibrational mode with frequency ω_i (or wavenumber $\bar{\nu}_i$), excited by a laser at frequency ω_L (or wavenumber $\bar{\nu}_L$) can be expressed as:[21,23,24]

$$\frac{d\sigma_{\mathrm{RS}}}{d\Omega} = C B_i^2 R_i \bar{\nu}_R^4 K(T), \tag{S16}$$

where $C = \pi^2/(45\epsilon_0^2)$ is a constant ($\epsilon_0 \equiv$ permittivity of free space= 8.8542 $10^{-12}\,\mathrm{Fm^{-1}}$), $\bar{\nu}_R = \bar{\nu}_L - \bar{\nu}_i$ [$\mathrm{m^{-1}}$] is the wavenumber of the Stokes-shifted Raman signal, B_i^2 [$\mathrm{kg\,m^2}$] is the square of the zero point amplitude of the normal mode in reduced mass coordinates, and R_i is the Raman scattering activity [$\epsilon_0^2\,\mathrm{m^4\,kg^{-1}}$]. The factor $K(T) = (1 - \exp(-hc\bar{\nu}_i/kT))^{-1}$ accounts for thermal population of the vibrational state. Furthermore, B_i^2 can be obtained from:

$$B_i^2 = \frac{h}{8\pi^2 c\bar{\nu}_i}. \tag{S17}$$

The Raman Activity R_i is a characteristic invariant upon arbitrary rotations of the Raman tensor of the probe. It can be expressed as:

$$R_i = 45\bar{\alpha}_i'^2 + 7\bar{\gamma}_i'^2 \tag{S18}$$

where $\bar{\alpha}'_i$ and $\bar{\gamma}'_i$ are the isotropic and anisotropic invariants of the Raman tensor $\underline{\alpha}'_i$ [$\epsilon_0\,\mathrm{m}^2\,\mathrm{kg}^{-1/2}$] of the vibrational mode.[21,25] In these standard definitions, the Raman tensor $\underline{\alpha}'_i$ corresponds to the derivatives of the electronic polarizability with respect to the reduced mass coordinates of a particular eigenvector representing a normal vibrational mode; thus resulting in the units of [$\epsilon_0^2\,\mathrm{m}^4\,\mathrm{kg}^{-1}$] for R_i, but it is commonly expressed in Gaussian units as [$\mathrm{Å}^4\,\mathrm{amu}^{-1}$]. Note that the Raman activity is one of the parameters in the output of DFT Raman computations for some of the most widely available programs at present like *Gaussian*[26] or *GAMESS*[27]. *It does not directly represent the relative intensities of the Raman peaks*, but can be used to predict them together with the absolute differential Raman cross-sections using Eq. S16. The depolarization ratio ρ_i of mode i can also be expressed in terms of the Raman tensor invariants as[21,25]:

$$\rho_i = \frac{3\bar{\gamma}_i'^2}{45\bar{\alpha}_i'^2 + 4\bar{\gamma}_i'^2}. \tag{S19}$$

All these definitions are standard Raman textbook material.

An additional aspect that needs special attention is that Eq. S16 is only valid for "isolated" (non-interacting) molecules *in vacuo*. If the sample under consideration is in the liquid state, at least two effects may affect this cross-section. The first is the possible interactions between molecules (either with the solvent in a diluted solution or with themselves at high concentrations). These effects are difficult to predict but may sometimes be guessed by comparing DFT predictions to experiments. The second is the *local field correction* due to the optical properties of the liquid. It is a well-understood effect in the framework of the optical properties of dielectric media; a correction factor for local fields must be applied to the Raman and every other optical susceptibility[28]. The local field felt by a molecule is modified compared to the macroscopic field (of Maxwell's equations) created by the laser excitation. For Raman scattering, this leads to a local field correction of the cross-section in Eq. S16 given by the factor[21,28]:

$$L = \left[\frac{\left(n^2+2\right)}{3}\right]^4, \tag{S20}$$

where n is the refractive index of the liquid (assumed here to be the same at both the excitation and Raman wavelengths, respectively: a good approximation for transparent liquids in the visible). This factor is usually not negligible. For example, $L = 2.5$ in water.

Finally, in a SERS context, it is often more convenient to consider the Raman polarizability tensor $\underline{\alpha}_i$ [$\epsilon_0\,\mathrm{m}^3$], rather than the Raman tensor $\underline{\alpha}'_i$. It directly relates the induced Raman dipole $\mathbf{p}_R$ to the local electric field $\mathbf{E}$ as $\mathbf{p}_R = \underline{\alpha}_i\mathbf{E}$. One can show that:

$$\underline{\alpha}_i = B_i\underline{\alpha}'_i, \tag{S21}$$

where B_i is defined in Eq. S17. We define the *magnitude of the Raman polarizability tensor* as

$$\alpha_0^2 = (45(\bar{\alpha})^2 + 7(\bar{\gamma})^2)/45, \tag{S22}$$

where $\bar{\alpha}$ and $\bar{\gamma}$ are the isotropic and anisotropic invariants of $\underline{\alpha}$. Averaging the emitted radiation of the induced Raman dipole over all possible orientations, we obtain an alternative expression for the cross-section as:

$$\frac{d\sigma_{\mathrm{RS}}}{d\Omega} = \frac{\omega_R^4\alpha_0^2}{16\pi^2\epsilon_0^2c^4}. \tag{S23}$$

This expression is equivalent to Eq. S16, but is more adequate to electromagnetic calculations of SERS enhancements, which rely on the concept of induced Raman dipole and Raman polarizability. The local field correction factor L, should also be applied here when relevant. One can also define the *normalized Raman tensor* as $\tilde{\underline{\alpha}} = \underline{\alpha}/\alpha_0$. This non-dimensional tensor characterizes the type of Raman tensor (its symmetry), independently of its strength characterized by the magnitude α_0. These definitions are useful in the context of SERS EFs.

D. Example of DFT computation of non-SERS cross-sections

The definitions and expressions of the previous section can now be used to determine Raman cross-sections, experimentally and theoretically. The experimental measurement of an absolute Raman cross-section is a difficult undertaking.[21] Such studies have been carried out for only a few substances, which then serve as standards. The relative cross-sections of other compounds are then easily measured and compared to the reference, from which the absolute cross-section is derived. It is therefore of paramount importance to make sure that the absolute cross-section of the reference is as accurate as possible.

To this end, we will first discuss the use of DFT calculations as a tool to estimate Raman cross-sections of small non-resonant molecules (which may be used as SERS probes or can simply serve as standards). Although several studies have compared the DFT predictions with experiments for the Raman frequencies,[2] few have in fact focused on the Raman intensities. Note that DFT predictions of Raman cross-sections cannot be trusted unless they are confirmed experimentally. This is because it is difficult to tell *a priori* whether resonant or pre-resonant contributions exist (which would then invalidate the semiclassical approach and therefore the DFT result; much more involved calculations, such as Time-dependent DFT, are then necessary[29]). The comparison of DFT predictions with experiments is still an instructive exercise, since when they agree: (*i*) it indicates that there are no contributions from resonance/pre-resonance effects, and (*ii*) it confirms independently the experimentally measured cross-section.

To illustrate this aspect, we show here that the DFT predictions compare well with experiments for some small

DFT predictions					Experimental			Reported (Ref. 21)	
$\bar{\nu}_i$	ρ_i	R_i	$\left(\frac{d\sigma}{d\Omega}\right)$	I_i^{Rel}	$\bar{\nu}_i$	ρ_i	I_i^{Rel}	$\left(\frac{d\sigma}{d\Omega}\right)$	I_i^{Rel}
cm^{-1}	[-]	[Å^4/amu]	[$10^{-32}\,\mathrm{cm}^2$/sr]	[-]	cm^{-1}	[-]	[-]	[$10^{-32}\,\mathrm{cm}^2$/sr]	[-]
265	0.75	0.49	25.9	0.16	280	0.70	0.17	-	-
293	0.26	8.97	130	0.82	302	0.26	0.85	144	0.85
509	0.18	23.7	159	1.00	516	0.16	1.00	169	1.00
800	0.63	14.3	53.4	0.34	806	0.60	0.26	44.0	0.26
1168	0.26	25.7	60.8	0.38	1143	0.32	0.34	-	-
1255	0.75	2.51	10.6	0.07	1237	0.74	0.04	-	-

TABLE S.II: Comparison of DFT predictions (gas phase), experimental measurements (liquid phase), and reported values (gas phase) for the different Raman active modes of 2-bromo-2-methylpropane (2B2MP), which is used later as a standard to obtain the cross sections of SERS probes. Absolute Raman cross-sections and relative intensities all relate to 633 nm laser excitation.

non-resonant molecules. The fact that the same absolute Raman cross-section can be independently obtained from both DFT and experiments gives an additional level of confidence in the values, which can therefore be used as a standard. Note that since DFT is used here as an additional validation procedure, its exact implementation (basis set, etc...) is not crucial and must be ultimately justified by its agreement with experimental results.

As an example, we focus in the following on the case of 2-bromo-2-methylpropane (a liquid at room temperature). This was selected as a possible standard as it is not too volatile and is non-toxic (although care must still be taken since it is flammable). Moreover, measurements of its absolute cross-section already exist in the literature[21] (in the gas phase). To confirm the validity of this standard, we performed DFT calculations using the Gaussian DFT package[26,30] with Becke's 3-parameter hybrid functional[31] and Lee-Yang-Parr[32] non-local electron correlation (commonly abbreviated as B3LYP) with basis set 6-311++G(d,p). A vibrational frequency analysis, which includes the Raman activity calculations, was carried out. We hence obtained the frequencies $\bar{\nu}_i$, Raman activities R_i, and depolarization ratios ρ_i for each peak, from which the gas-phase Raman cross-section at 633 nm can be calculated using Eq. S16. A local field correction factor of $L = 3.3$ (index of refraction $n = 1.428$ for 2-bromo-2-methylpropane) is then applied to obtain the predicted liquid-phase cross-sections. The DFT predictions are summarized in Table S.II.

We also measured experimentally the peak frequencies $\bar{\nu}_i$, relative intensities I_i^{Rel}, and depolarization ratios ρ_i. For small molecules like this one, the predicted peak frequencies are in fairly good agreement with experiments, thus allowing easy matching of the peaks between DFT predictions and experiments. The next step to ensure that the DFT predictions are consistent is to compare the predicted depolarization ratios and relative intensities with experiments. Any large discrepancies could be an indication that the DFT predictions fail, for example because of resonance effects or strong inter-molecular interactions. As seen in Table S.II, the agreement is extremely good, which indicates that the DFT predictions are fairly accurate for this compound. This implies that the predicted absolute Raman cross-section should also be reliable. For this compound, where such measurements have been reported in the past[21], we can also check (see Table S.II) that this is indeed the case in the gas phase.

This agreement between DFT and experiments strongly reinforces the confidence in the value of the absolute Raman cross-section at 633 nm for this compound. It can also be used as a reference at longer wavelengths, where no additional resonance can appear and the cross-section can also be predicted accurately. The liquid-phase absolute Raman cross-section can be directly deduced from the DFT calculation with a local field correction factor of $L = 3.3$. 2-bromo-2-methylpropane (2B2MP) was therefore selected as a standard to determine the cross-sections of other liquids, using as a reference the $516\,\mathrm{cm}^{-1}$ peak with a reference absolute differential cross-section of $d\sigma/d\Omega = 5.4 \times 10^{-30}\,\mathrm{cm}^2$ /sr at 633 nm.

The validity of this reference was inferred from the agreement between DFT predictions and (*i*) reported gas-phase absolute Raman cross-section measurements, (*ii*) measured relative Raman intensities and depolarization ratios of the main peaks in the liquid phase. As an additional validation step, we measured using this reference the non-SERS absolute cross-sections of several liquids with reported values in the literature[21]. For as long as the exact same experimental conditions are used, the absolute cross-section of a sample can be determined from the relative concentrations and measurement of the peak intensities of the reference and sample from:

$$\left(\frac{d\sigma_{\mathrm{RS}}}{d\Omega}\right)_{\mathrm{Sample}} = \left(\frac{d\sigma_{\mathrm{RS}}}{d\Omega}\right)_{\mathrm{Ref}} \cdot \frac{I_{\mathrm{Sample}}}{I_{\mathrm{Ref}}} \cdot \frac{c_{\mathrm{Ref}}}{c_{\mathrm{Sample}}}, \quad \text{(S24)}$$

where c and I are the concentrations and measured integrated peak intensities, respectively. The results for several liquid compounds are shown in Table S.III along with previously reported cross-section values.[21,33] The DFT predictions for these compounds are also shown to further illustrate the predictive power of DFT in terms of absolute Raman cross-sections. The general agreement between the measured and reported values confirms the validity of our reference compound.

	$\bar{\nu}_i$ [cm^{-1}]	$\left(\frac{d\sigma}{d\Omega}\right)$ [10^{-30} $\mathrm{cm}^2\mathrm{sr}^{-1}$]		
	meas.	meas.	rep.	DFT
Benzene	992	8.3	7.9	8.8
Toluene	1002	2.9	3.5	3.8
Dichloro-	282	1.7	1.9	3.1
methane	713	2.9	3.1	2.3

TABLE S.III: Comparison of the absolute Raman cross section of common liquid reference compounds obtained from: (meas.) our measurements using the $516\,\mathrm{cm}^{-1}$ mode of 2B2MP as a reference; (rep.) reported values[21,33]; and (DFT) obtained from DFT calculations with a local field correction factor as defined in Eq. S20. The discrepancy between DFT and experiments for Dichloromethane is attributed to strong intermolecular interactions. The fact that our measurements are either above (benzene) or below (toluene) reported values indicates that our reference is a good compromise amongst the existing standards. It also highlights the experimental difficulties in measuring accurately absolute cross-sections and the unavoidable uncertainties in the reported values in the literature. For these reasons, we believe that the DFT predictions may sometimes provide an additional level of confidence in a given standard.

E. Practical estimation of non-SERS cross-sections of SERS probes

Now the reference compound 2B2MP has been characterized in detail, and its reference Raman cross-section validated by various means, it remains to use it toward its original goal: the measurement of the Raman (non-SERS) cross-section of representative SERS probes. Four probes have been selected (RH6G, CV, BTZ, and BTA) and their properties are discussed in Sec. III.A of the main paper. The results are also presented and discussed in the main paper. We here only give a few extra details about the actual experimental procedure, including the actual Raman spectra (shown in Fig. S1).

A Jobin-Yvon LabRam Raman microscope with a $\times 100$ Olympus water immersion objective (N.A. 1.0) was used for excitation and collection in a standard backscattering configuration. Excitation was provided by a 633 nm HeNe laser, with a power of $\sim 4.5\,\mathrm{mW}$ at the sample. Prior to each measurement, the reference 2-bromo-2-methylpropane (2B2MP) was measured under the same experimental conditions. Solutions (in water) of RH6G, CV, BTZ, and BTA, were measured using integration times in the range $150-400\,\mathrm{s}$. The obtained spectra are shown in Fig. S1. Selected peaks from the spectra of the dyes were then fitted using pseudo-Voigt functions, and the integrated intensity was compared to that of the reference $516\,\mathrm{cm}^{-1}$ peak of 2-bromo-2-methylpropane using Eq. S24 with $c_{\mathrm{Ref}} = 8.76\,\mathrm{M}$. There are at least two potential sources of problems in such measurements. The first is the possible optical absorption of the dye sample (especially at high concentrations), which would affect the results. To ensure this was not an issue here, we chose a lower concentration for CV (most absorbing at 633 nm) and repeated the measurements at two concentrations for CV (10 and 20 μM) and RH6G (50 and 100 μM). The second is the possibility of dye photobleaching. In a liquid, dye diffusion is fast and one could expect it to be much faster than photobleaching time, but to make sure this was not an issue, we also repeated the measurements at half the laser intensity. These issues are irrelevant for BTA and BTZ and concentrations of 100 mM and 1 mM, respectively, were used. As shown in Fig. S1, the Raman spectra are of sufficient quality to extract reliable integrated intensities. The measured absolute Raman cross-sections for the main Raman peaks of these four compounds are summarized in Table I of the main paper.

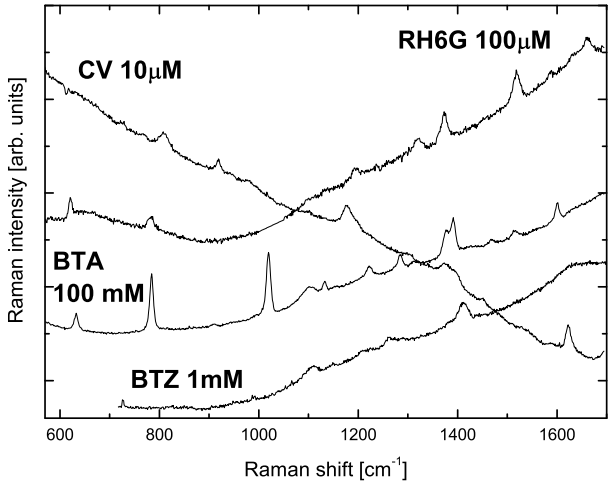

FIG. S1: Raman (non-SERS) spectra from the analytes characterized here (various concentrations, c, and integration times IT): CV, $c = 10\,\mu$M, IT= 150 s; RH6G, $c = 100\,\mu$M, IT= 400 s; BTA, $c = 100$ mM, IT= 240 s; BTZ, $c = 1$ mM, IT= 300 s. These are raw spectra, only offset vertically to fit in the same figure. The background for RH6G, BTA, and BTZ resembles that obtained from a water sample. A small amount of fluorescence is observed for CV but this does not prevent the obtention of the Raman spectrum.

S.IV. CHARACTERIZATION OF THE SCATTERING VOLUME

A. Introduction

In many measurements, we simply compare Raman signals of two solutions under exactly the same conditions. The cross-section of one can then be deduced from that of the other provided the concentrations of the samples are known. This is the method we have used to measure the absolute cross-section of dyes in the previous Section. In this approach, the details of the excitation beam profile and detection are irrelevant: for as long as the same experimental conditions are kept, the results are directly comparable.

This is no longer the case, however, when estimating the SERS enhancement factors for single molecules. In this case, SM-SERS events are first identified, for example, via the BiASERS method[34]. Some of these may originate from colloids/molecules located at the periphery of our scattering volume and, accordingly, are not subject to the maximum power excitation density. To eliminate these, we typically only consider the strongest SM events, for which the single molecule was at an optimum position within our beam (i.e. at the center of the focal plane). In order to estimate the absolute cross-section for this event, the SERS signal $I^{\mathrm{SM}}_{\mathrm{SERS}}$ [W] must be compared to the average Raman signal of one reference molecule $\langle I^{\mathrm{SM}}_{\mathrm{Ref}}\rangle$ [W] at the center of the focal plane under the same experimental conditions.

However, experimentally, we only have access to the total Raman signal $I^{\mathrm{Tot}}_{\mathrm{Ref}}$ from many reference molecules with concentration c. It is therefore necessary to precisely characterize our scattering volume (excitation and collection) to relate this to the desired quantity $\langle I^{\mathrm{SM}}_{\mathrm{Ref}}\rangle$.

B. General principle

We shall in the following consider our specific setup, but the arguments can be easily adapted to other configurations in the sense that we only use concepts of confocal microscopy that should be adaptable to other systems. The scattering volume is characterized by two distinct, but intertwined, aspects. The first is the excitation intensity profile, $I(\rho,z)$ [$\mathrm{W\,m^{-2}}$](axial symmetry is assumed here), i.e. the laser intensity as a function of position, which is inevitably non-uniform. The second aspect is the detection efficiency profile $\eta(\rho,z)$. This can be strongly dependent on the experimental setup. Our system consists of a confocal setup where the collected light goes through a square confocal pinhole, which also serves as an entrance slit for the monochromator. Only light emitted from a point source at the center of the focal plane is detected with maximum efficiency η_0.

Assuming $I(\rho,z)$ and $\eta(\rho,z)$ are known, it is then a simple matter to calculate the Raman intensity of our reference with concentration c [M or $\mathrm{mol\,m^{-3}}$] and differential cross-section $d\sigma/d\Omega$ [$\mathrm{m^2/sr}$]. The collecting angle is $\delta\Omega$ [sr] and we define for simplicity $\sigma_d = (d\sigma/d\Omega)\delta\Omega$ [$\mathrm{m^2}$], which leads to:

$$I^{\mathrm{Tot}}_{\mathrm{Ref}} = cN_a\sigma_d \int_{\rho=0}^{\rho=\infty} 2\pi\rho \int_{z=-\infty}^{z=+\infty} I(\rho,z)\eta(\rho,z)d\rho dz, \tag{S25}$$

where $N_a = 6.02\times10^{23}$ is Avogadro's number [$\mathrm{mol^{-1}}$]. We can also estimate the Raman intensity of one single reference molecule at the center of the focal plane:

$$\langle I^{\mathrm{SM}}_{\mathrm{Ref}}\rangle = \sigma_d I_0 \eta_0 \tag{S26}$$

This can therefore be deduced from the (measurable) $I^{\mathrm{Tot}}_{\mathrm{Ref}}$ as:

$$\langle I^{\mathrm{SM}}_{\mathrm{Ref}}\rangle = \frac{I^{\mathrm{Tot}}_{\mathrm{Ref}}}{cN_aV_{\mathrm{eff}}}, \tag{S27}$$

where an effective scattering volume V_{eff} [$\mathrm{m^3}$] has been defined as:

$$V_{\mathrm{eff}} = \int_{\rho=0}^{\rho=\infty} 2\pi\rho \int_{z=-\infty}^{z=+\infty} \frac{I(\rho,z)}{I_0}\frac{\eta(\rho,z)}{\eta_0}d\rho dz. \tag{S28}$$

V_{eff} corresponds to the volume from which the same Raman signal would be observed *if the excitation and detection efficiency were both uniform* and equal to their maximum values, I_0 and η_0. Note that V_{eff} is smaller than the actual volume probed by our system. This approach is an extension to that described in Ref. 17, where an effective height was defined to characterize the detection efficiency (non-uniform excitation was then ignored).

In all experiments, $I(\rho,z)$ and $\eta(\rho,z)$ will be intertwined and appear as a product (as in the expression above). Their respective effects can however be deconvoluted because $\eta(\rho,z)$ can be varied independently of $I(\rho,z)$ in the detection setup (by changing the confocal pinhole or slit sizes).

We now focus on some of the techniques available to characterize and measure the effective scattering volume. While this could be argued to be a special topic of confocal microscopy, it is an essential step in the SMEF problem and it is therefore necessary to show its details in full for future applications and to reproduce our experimental SMEFs values independently. Our approach here is to present the simplest approximations, which still capture most of the important aspects of the problem. More elaborate treatments can be found in specialized textbook.[35] We conclude at the end of this section with a subsection on how these ideas of confocal microscopy apply to the single molecule EF problem.

C. Excitation profile

To determine the excitation, it will first be approximated by a Gaussian beam profile with axis along z.

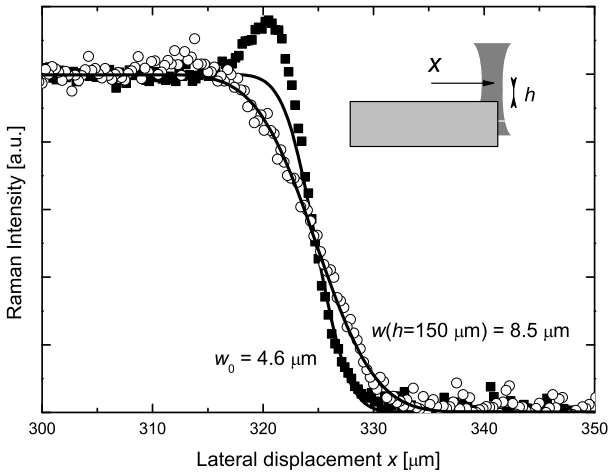

FIG. S2: Raman signal from silicon at 633 nm as a function of displacement while scanning over a Si substrate edge. A $\times$10 microscope objective with N.A. of 0.25 was used here. Symbols correspond to experimental values at laser focus on the Si substrate (solid squares) and at a distance $f = 150\,\mu$m beyond focus (open circles). Solid lines are fits to the data. The overshoot observed when reaching the Si edge is not taken into account for the fits.

Following standard definitions,[36,37] the intensity profile is therefore

$$I(\rho, z) = I_0 \frac{w_0^2}{w(z)^2} \exp(-\frac{2\rho^2}{w(z)^2}), \tag{S29}$$

where I_0 [W m^{-2}] is the intensity at the center of the focal plane, w_0 [m] is the waist of the Gaussian beam and

$$w(z) = w_0 \sqrt{1 + \frac{z^2}{z_0^2}} \quad \text{, where} \quad z_0 = \frac{\pi w_0^2}{\lambda}. \tag{S30}$$

The power P_0 [W] of such a Gaussian beam is:

$$P_0 = \frac{\pi w_0^2}{2} I_0. \tag{S31}$$

Since P_0 is easily measured (with a power meter), the only unknown parameter is the waist w_0.

D. Detection efficiency profile

The detection efficiency profile may be more system-specific. Laterally, it will be mainly determined by the shape and size of the entrance slits of the monochromator. An image of the spot area is formed on this aperture, and in a first approximation, the part of this image that is inside the aperture will go through and be detected while the rest is simply cut out. This ignores diffraction effects, which is almost always correct since most spectrometers magnify the size of the real spot on the entrance slit. The dimensions of the image on the slit is related to the actual dimensions at the sample by a factor X, which is the magnification factor of the microscope objective times any other magnifications introduced by the collecting optics (this is setup-dependent, it adds a factor 0.56 $\times$ the magnification of the objective in our case, resulting in a factor $X = 56$ for a $\times$100 objective). We restrict ourselves here to our specific setup, where the slits form a square aperture[38] of dimension $2L$ [m] (edge length). The detection efficiency is therefore of the form:

$$\eta(x, y, z) = \eta_\perp(z) \quad \text{if} - L/X \le x, y \le L/X,$$
$$\eta(x, y, z) = 0 \quad \text{otherwise.} \tag{S32}$$

The axial detection efficiency $\eta_\perp(z)$ also depends strongly on the optical setup, in particular wavelength, microscope objective, and confocal pinhole size. It is maximum at $z = 0$ and decreases away from the focal plane. In a confocal setup, this decrease can be over a very small distance characterized by the confocal depth.

Within these assumptions it is also possible to simplify the integrals in Eqs. S25 and S28 *when the entrance slit is sufficiently open*. More precisely, if $L \gg w_0\, X$, then only a negligible part of the image of the Gaussian beam excitation is cut out by the slits, and the effect of the lateral detection efficiency can then be ignored. In this case the signals are independent of L for as long as L is sufficiently large. This condition is most likely met when the slits are fully open and is easy to check experimentally, since the signal should not change when the slits are being closed (up to a point where this approximation is no longer valid). For example, in measuring the Raman signal from 2-Bromo,2-methylpropane (2B2MP) at 633 nm using the $\times$100 (N.A. 1.0) water immersion objective, the signal remains constant (within 2.5%) when closing the slits from $L = 354\,\mu$m (pinhole of 1000 μm) to $L = 212\,\mu$m (pinhole of 600 μm). In this case, the ρ dependence of η can be ignored, and the integral over ρ in Eqs. S25 and S28 becomes independent of z and simply equals to P_0, the incident power. This leads us to introduce an effective height, H_{eff} [m], defined as

$$H_{\text{eff}} = \int_{z=-\infty}^{z=+\infty} \frac{\eta_\perp(z)}{\eta_0}\, dz. \tag{S33}$$

The equations then simplify to:

$$I_{\text{Ref}}^{\text{Tot}} = c\sigma_d P_0 H_{\text{eff}}, \tag{S34}$$

and

$$V_{\text{eff}} = A_{\text{eff}} H_{\text{eff}}, \quad \text{where} \quad A_{\text{eff}} = P_0/I_0 = \frac{\pi w_0^2}{2} \tag{S35}$$

is the effective surface area [m^2] of the Gaussian excitation. This generalizes the concept of effective height of the scattering volume, introduced in Ref. 17, to the common case of non-uniform (Gaussian) excitation. It is important to note however that this approach is only valid when the entrance slits are sufficiently open, which

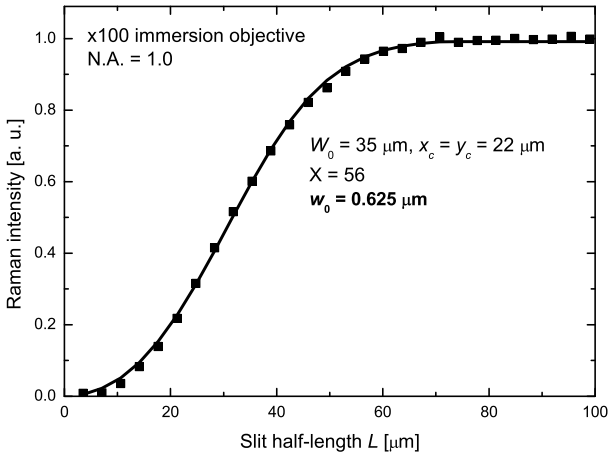

FIG. S3: Raman signal from a Si substrate at 633 nm as a function of entrance slits sizes. A ×100 immersion (water) microscope objective with N.A. of 1.0 was used here and an additional scaling factor of 0.56 exists for our particular optical setup, resulting in a magnification of $X = 56$ from sample to its image at the square aperture of the entrance slits. Symbols correspond to experimental values at laser focus on the Si substrate and the solid line is a fit to the data using Eq. S37.

allows one to "factorize" (deconvolve) the respective contributions of excitation and detection. As discussed later, it is no longer valid for smaller slits and will therefore fail in a truly confocal regime. H_{eff} cannot be simply viewed as the confocal depth of the microscope.

Having defined more accurately the excitation profile and detection profile, we now review a few methods that can be used to measure their respective characteristics, and in particular w_0 (and therefore A_{eff}) for excitation, and $\eta_\perp(z)$ (and therefore H_{eff}) for detection.

E. Scan over an edge

One simple approach to determine the waist of the excitation profile is to measure the Raman signal of a strongly absorbing thin film (typically silicon) as the objective is focused on the film and scanned laterally over a sharp (cleaved) edge (scanning knife-edge method[39]) as shown schematically in Fig. S2. Because of strong absorption, all the Raman signal comes from the Si wafer surface (and therefore from the focal plane $z = 0$). The first step is to ensure that the slits are sufficiently open to collect all the signal from the laser spot. This can easily be checked since the Raman signal will remain constant when closing the slits if this condition is fulfilled. We are then in a situation where the detection efficiency is uniform (no lateral restriction by the slits, and no z dependence since all the signal comes from the focal plane).

Assuming we scan the spot along the x axis and that the edge is at $x = x_0$ (silicon wafer on $x < x_0$), the Raman intensity dependence is then:

$$I(x) = \frac{I_{\max}}{2}\left[1 + \text{erf}\left(\frac{\sqrt{2}(x_0 - x)}{w_0}\right)\right], \qquad \text{(S36)}$$

where $\text{erf}(x)$ is the error function. This intensity profile is quite sensitive to the value of w_0, and this parameter can therefore be extracted from a fit to the experimental data. An example is shown in Fig. S2. Note that there is a slight overshoot of the signal as we reach the Si edge; this is purely an "edge" effect to do with the additional contribution from the diffracted beam on the side of the wafer when the beam is half-way through the edge: this effect can be ignored when fitting to the above expression. For a ×10 objective as in our example, a waist of $w_0 = 4.6\,\mu$m is derived. The same experiment can also be done out of focus ($h = 150\,\mu$m beyond focus in the example of Fig. S2). The derived waist is then $w(h) \approx 8.5\,\mu$m, which for a Gaussian beam can also be predicted from Eq. S30 to be $w(h) = 8\,\mu$m, in good agreement with the measured value.

This technique, although fairly accurate presents at least two shortcomings. Firstly, it is necessary to have scanning capabilities on the Raman system (Raman mapping), and secondly, its accuracy decreases substantially for narrowly focused beams, typically for $w_0 < 2\,\mu$m. It is in fact unpractical for high magnification, high N.A. objectives with near-diffraction-limited spot sizes.

F. Slit size dependence

An alternative method is to use, instead of an edge on the sample, the monochromator's slits (which in our system is the confocal pinhole at the same time) as a spatial filter. The main advantage here is that the spatial filtering is carried out on the image, which is much larger, and not on the sample itself where diffraction or accurate positioning may cause problems. When closing the slits in a controlled way, an increasing part of the spot image is cut out from detection, and the signal decreases correspondingly. The experimental conditions are the same as before, i.e. at focus, $z = 0$, on a Si substrate to avoid any influence of the z-dependence.

Again, we restrict ourselves here to our specific setup, where the slits form a square aperture of dimension $2L$. An image of the Gaussian excitation, with waist $W_0 = w_0 X$, is formed in this aperture and centred on $x = 0, y = 0$. The waist of the image W_0 is related to the actual waist of the beam by the magnification factor X, as explained before. We will allow for a possible (almost always present) slight misalignment, which means that the aperture may be slightly off-center, at $x = x_c, y = y_c$ compared to the beam image. The dependence of the Raman intensity with slit size (characterized by L) can then be predicted by integrating the intensity profile of

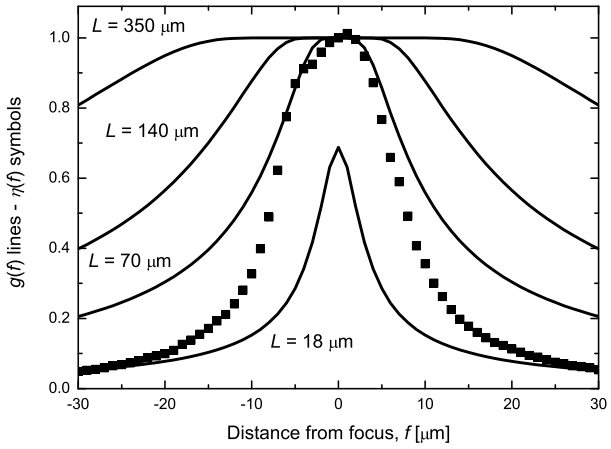

FIG. S4: Raman intensity from a Si substrate at 633 nm as a function of distance f from the focal plane (symbols). A ×100 immersion (water) microscope objective with N.A. of 1.0 was used here and the slits were fully opened ($L = 354\,\mu$m). The solid lines show the function $g(f)$ obtained from Eq. S40 for 4 representative slit sizes. For the largest slit size, $g(f)$ remains nearly constant in the range of interest, and the symbols are therefore a faithful representation of the axial detection efficiency profile $\eta_\perp(f)$.

the beam image within the aperture, and is given by:

$$\frac{I(L)}{I_{\max}} = \frac{1}{4}\left[\mathrm{erf}\left(\frac{\sqrt{2}}{W_0}(x_c+L)\right) - \mathrm{erf}\left(\frac{\sqrt{2}}{W_0}(x_c-L)\right)\right] \times \left[\mathrm{erf}\left(\frac{\sqrt{2}}{W_0}(y_c+L)\right) - \mathrm{erf}\left(\frac{\sqrt{2}}{W_0}(y_c-L)\right)\right]. \quad \text{(S37)}$$

This expression simplifies for a perfect alignment to:

$$\frac{I(L)}{I_{\max}} = \left[\mathrm{erf}\left(\frac{\sqrt{2}L}{W_0}\right)\right]^2. \quad \text{(S38)}$$

Similar expressions could be obtained for circular or rectangular apertures.

As for the scan-over-an-edge technique, the above expressions can be fitted to experimental data to derive W_0 with good accuracy. In fact, for the example already shown in Fig. S2, the slit dependence gives the same w_0 as that obtained from the scan-over-the-edge method (within experimental errors). Fig. S3 shows another example for the ×100 N.A.=1.0 water immersion objective, for which the scan-over-an-edge technique would fail. A waist of $w_0 \approx 0.625\,\mu$m is deduced. A slight misalignment is also evidenced here with $x_c = y_c = 22\,\mu$m.

G. Axial detection efficiency

Once w_0 is determined, the excitation profile is fully characterized and we can now focus on the axial detection efficiency $\eta_\perp(z)$. A standard approach here is to measure the Si Raman signal $I(f)$ as a function of distance f from the focal plane on the substrate.[17] A bell-shaped profile is obtained, whose FWHM is defined as the confocal depth. However, concluding that this profile corresponds to the axial detection efficiency $\eta_\perp(z)$ can be erroneous for at least one reason: the size of the illuminated area on the Si substrate increases when going away from or beyond focus (due to the Gaussian beam profile). The periphery of this area may then be cut out from detection because of the lateral detection efficiency (which depends on the entrance slit size). Because of this, a bell-shaped curve can be obtained from $I(f)$ even if $\eta_\perp(z)$ was constant. It is therefore necessary to deconvolve this effect from the actual contribution of $\eta_\perp(z)$, or at least ensure that it does not play a role. If we neglect the finite penetration depth into Si, all the Raman signal comes from the Si surface at $z = f$ and we then have for a given slit size L, $I(f, L) = I_{\max}\eta_\perp(f)g(f, L)$ with

$$g(f, L) = \int_{x=-L}^{x=L}\int_{y=-L}^{y=L} dxdy\, I(x, y, f)/I_{\max}. \quad \text{(S39)}$$

$g(f, L)$ contains contributions from both the non-uniform excitation and the lateral detection efficiency (governed by the slit size L). It can moreover be calculated from Eq. S37, or in the case of ideal alignment from Eq. S38:

$$g(f, L) = \left[\mathrm{erf}\left(\frac{\sqrt{2}L}{Xw(f)}\right)\right]^2, \quad \text{(S40)}$$

where $w(f)$ is given in Eq. S30. The function $g(f, L)$ is precisely the origin of the problem discussed above. If this function is not constant, then $I(f)$ does not directly reflect the axial detection efficiency, but a convolution of it with a complex function of excitation profile and lateral detection efficiency.

We illustrate this on the specific example of interest to the main paper, where a ×100 N.A.=1.0 water immersion objective is used at 633 nm. The magnification factor between spot and image is then $X = 56$. The waist of the Gaussian beam excitation has been measured before: $w_0 = 0.625\,\mu$m, corresponding to a waist of $W_0 = X\,w_0 = 35\,\mu$m in the image. Examples of the profile of $g(f)$ for these parameters, calculated from Eq. S40, are given in Fig. S4 for different slit sizes L. It is clear from these that for the smallest slit sizes, a bell-shaped curve is already obtained from $g(f)$ and is not a result of the axial detection profile. This effect must be taken into account for an accurate determination of the confocal profile. For the largest slit size, however, $g(f)$ remains almost constant over a wide range of distances. In this case, the slits are sufficiently open not to cut out any of the signals emitted from the scattering volume. This is the same conclusion as that reached earlier; the lateral detection efficiency does not influence the signals for this objective and fully open slits. It is also clear in Fig. S4 that the effect of the lateral detection efficiency can become very important at smaller slit sizes. In this case, $I(f)$ is not a truthful representation of $\eta_\perp(f)$.

What we need for our purpose here is the best possible characterization of the scattering volume. From the previous arguments, this is more easily achieved when the slits are fully opened since $g(f) \approx 1$ and has only a negligible effect. In this case, $I(f) \propto \eta_\perp(f)$ is a faithful representation of the axial detection efficiency. The experimental curve $I(f)$ ($\propto \eta_\perp(f)$) is also shown in Fig. S4 for the confocal pinhole fully opened ($H = 1000\,\mu$m) corresponding to a slit half-size of $L = 354\,\mu$m. From this profile, it is straightforward to compute the effective height defined in Eq. S33: $H_{\text{eff}} \approx 21.3\,\mu$m. If the (small) correction introduced by $g(f)$ is taken into account, we obtain $H_{\text{eff}} \approx 21.1\,\mu$m.

Finally, $\eta_\perp(f)$ exhibits a full width at half maximum (FWHM) of the order of $\Gamma = 15\,\mu$m. It is interesting to remark that the curve $I(f)$ narrows to a FWHM of about $9\,\mu$m when decreasing the pinhole size to $H = 50\,\mu$m (slits of $L = 18\,\mu$m). This could at first be attributed to a reduced width for $\eta_\perp(f)$, but a more careful analysis shows that it can be explained by an unchanged $\eta_\perp(f)$ convoluted with the function $g(f)$ for this slit size (see Fig S4). This implies the confocal pinhole is still too large for the setup to operate in a truly confocal regime, and we simply observe the combined effect of Gaussian excitation with limited lateral detection (modeled by $g(f)$), and not the axial detection profile. This also shows that, unlike many results reported in the literature, a very careful characterization of the scattering volume is required if the claim of truly confocal Raman spectroscopy is to be made and that many manufacturer settings may not operate in a truly confocal mode.

H. Single Molecule cross-section

Using the results from this careful characterization of the scattering volume, we are now in a position to estimate the effective scattering volume, required for the calibration of single molecule cross-sections.

For the experimental setup used in this work ($\times$100 immersion lens with N.A. of 1.0 at 633 nm), the excitation profile is a Gaussian beam with waist $w_0 = 0.625\,\mu$m, corresponding to an effective area $A_{\text{eff}} = 0.61\,\mu\text{m}^2$. The lateral detection efficiency is given in Eq. S32, but for fully opened slits, its effect is in fact negligible. The axial detection efficiency is shown in Fig. S4 and the corresponding effective height is $H_{\text{eff}} \approx 21\,\mu$m. From Eq. S35, we deduce an effective scattering volume of $V_{\text{eff}} \approx 13\,\mu\text{m}^3$.

As mentioned in the introduction of this Appendix, in order to determine the SMEF (or apparent cross-section) for a given SM-SERS event, one needs to compare the SM-SERS signal $I^{\text{SM}}_{\text{SERS}}$ to the average Raman signal of a single reference molecule $\langle I^{\text{SM}}_{\text{Ref}}\rangle$ under the exact same conditions. By choosing only the strongest SM-SERS events, we ensure that they correspond to a molecule at the center of the focal plane, where the excitation density and collection efficiency are maximum, i.e. I_0 and η_0, respectively. Only the total signal $I^{\text{Tot}}_{\text{Ref}}$ of a large concentration of reference molecules is measurable in practice. This must be measured under experimental conditions where the scattering volume can be accurately characterized, i.e. with slits fully open, so that $\langle I^{\text{SM}}_{\text{Ref}}\rangle$ can be deduced from Eq. S27.

To this end, after all SM-SERS experiments, a sample of pure 2-bromo,2-methylpropane (2B2MP) is measured under those experimental conditions for which $V_{\text{eff}} \approx 13\,\mu\text{m}^3$ was determined. As an example, for the BiASERS experiments presented in the main paper, the $516\,\text{cm}^{-1}$ mode of 2B2MP had a total Raman intensity of $I^{\text{Tot}}_{\text{Ref}} = 1.7\times10^4$ cts/s. The concentration of pure 2B2MP is $c = 8.76\,$M, so according to Eq. S27, a single molecule of 2B2MP at the center of the beam has a reference average Raman intensity of $\langle I^{\text{Ref}}_{\text{SM}}\rangle = 2.5\times10^{-7}$ cts/s. This estimate can then be compared to the SM-SERS signals of a single dye in the BiASERS method to derive the SMEF and the corresponding SERS differential cross-section.

S.V. MEASURING THE SMEF USING TEMPERATURE-DEPENDENT VIBRATIONAL PUMPING

The samples were prepared as described in Ref. 13, resulting in large Ag-colloid cluster aggregates. A $\times$10 objective was used for excitation and collection. A low magnification objective is advantageous here, since it enables us to probe a larger area (therefore removing any effect of the non-uniformity of the sample), and also ensures the excitation density is low enough to avoid any photobleaching of the analytes. One of the most important parameter for TDVP is the maximum excitation density (at the centre of the exciting beam). This was measured accurately using the "scan-over-an edge" method (see Sec. S.IV). For RH6G, the excitation density was $I_0 = 9.0\times10^3\,\text{W cm}^{-2}$. The larger SERS cross-sections for CV peaks enabled us to use a lower excitation density of $I_0 = 6.4\times10^2\,\text{W cm}^{-2}$. Fig. S5 shows the pumping curves obtained for 4 modes of RH6G, along with fits to the data following the model described in Refs. 13,14. The cross-sections were derived from the fits, using the corrected lifetime method as described in Ref. 13 (the reference peak was $1364\,\text{cm}^{-1}$ for RH6G, and $1175\,\text{cm}^{-1}$ mode for CV). The results are compiled in Table III of the main paper. Note that the pumping cross-sections cannot be readily compared to the non-SERS cross-sections to obtain the SMEF for two reasons: Firstly, they correspond to a statistical average, heavily biased towards the largest cross-sections[13] exhibited by the SERS substrate. For a collection of SERS hot-spots, this was shown[40] to be approximately half the maximum cross-section. Secondly, the pumping cross-section is a *total* SERS cross-section. In order to deduce from it, the *differential* SERS

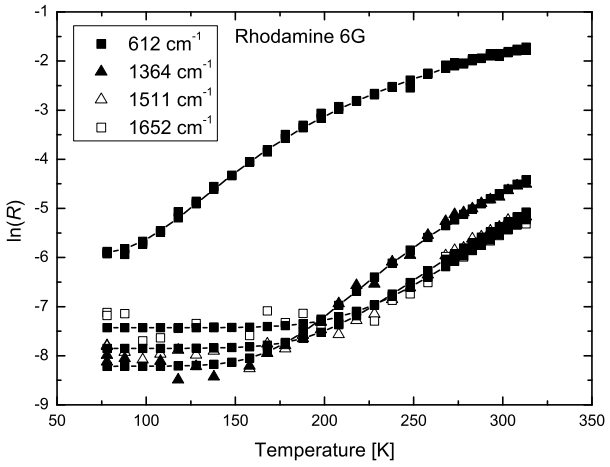

FIG. S5: The natural logarithm of the anti-Stokes to Stokes ratio (R) is measured as a function of temperature (T) for different Raman modes of RH6G. The solid lines are fits with the theoretical model of Ref. 13. The curves show a characteristic shape approaching a plateau at low temperatures which differentiates a "thermally dominated" regime at high T's from a "pumping dominated" regime at low T's. From these pumping curves, estimates of the maximum achievable SERS cross sections on the substrate can be obtained following the methods described in detail in Refs. 13,14.

cross-section, we must first assume that the non-radiative contribution is negligible compared to the radiative part. This approximation is in fact implicit in the use of the corrected lifetime method. We believe it is a reasonable approximation for a hot-spot (which must have a large radiative enhancement). Moreover, by integrating the differential SERS cross-section at a hot-spot over all possible emission directions, one can show there is a factor $8\pi/3$ between differential and integrated radiative SERS cross-section at the hot-spot. With these corrections, the maximum differential SERS cross-section $d\sigma_{\rm SERS}/d\Omega$ on the substrate can be deduced from the pumping cross-section $\sigma_{\rm pump}$ using the relation:

$$\frac{d\sigma_{\rm SERS}}{d\Omega} \approx \frac{3}{4\pi}\sigma_{\rm pump}. \qquad \text{(S41)}$$

From there the maximum SMEF can be deduced as before, taking into account the non-SERS cross-sections derived before. These are summarized in Table III of the main paper for RH6G and CV.

* Electronic address: Eric.LeRu@vuw.ac.nz
† Electronic address: Pablo.Etchegoin@vuw.ac.nz

[1] Le Ru, E. C.; Etchegoin, P. G. *Chem. Phys. Lett.* **2006**, *423*, 63.
[2] Aroca, R. *Surface Enhanced Vibrational Spectroscopy*; Wiley: Chichester, 2006.
[3] Persson, B. N. J.; Zhao, K.; Zhang, Z. *Phys. Rev. Lett.* **2006**, *96*, 207401.
[4] Le Ru, E. C.; Etchegoin, P. G. *Phys. Rev. Lett.* **2006**, *97*, 199701.
[5] Persson, B. N. J.; Zhao, K.; Zhang, Z. *Phys. Rev. Lett.* **2006**, *97*, 199702.
[6] Lombardi, J. R.; Birke, R. L.; Lu, T.; Xu, J. *J. Chem. Phys.* **1986**, *84*, 4174.
[7] King, F. W.; Duyne, R. P. V.; Schatz, G. C. *J. Chem. Phys.* **1978**, *69*, 4472.
[8] Efrima, S.; Metiu, H. *J. Chem. Phys.* **1979**, *70*, 1602.
[9] Weber, W. H.; Ford, G. W. *Phys. Rev. Lett.* **1980**, *44*, 1774.
[10] Ford, G. W.; Weber, W. H. *Physics Rep.* **1984**, *113*, 195.
[11] Lal, S.; Grady, N. K.; Goodrich, G. P.; Halas, N. J. *Nano Lett.* **2006**, *6*, 2338.
[12] Moskovits, M. *J. Chem. Phys.* **1982**, *77*, 4408.
[13] Maher, R. C.; Cohen, L. F.; Le Ru, E. C.; Etchegoin, P. G. *J. Phys. Chem. B* **2006**, *110*, 19469.
[14] Maher, R. C.; Etchegoin, P. G.; Le Ru, E. C.; Cohen, L. F. *J. Phys. Chem. B* **2006**, *110*, 11757.
[15] Félidj, N.; Aubard, J.; Lévi, G.; Krenn, J. R.; Salerno, M.; Schider, G.; Lamprecht, B.; Leitner, A.; Aussenegg, F. R. *Phys. Rev. B* **2002**, *65*, 075419.
[16] McFarland, A. D.; Young, M. A.; Dieringer, J. A.; Duyne, R. P. V. *J. Phys. Chem. B* **2005**, *109*, 11279.
[17] Cai, W. B.; Ren, B.; Li, X. Q.; She, C. X.; Liu, F. M.; Cai, X. W.; Tian, Z. Q. *Surf. Sci.* **1998**, *406*, 9.
[18] Hildebrandt, P.; Stockburger, M. *J. Phys. Chem.* **1984**, *88*, 5935.
[19] Su, K.-H.; Durant, S.; Steele, J. M.; Xiong, Y.; Sun, C.; Zhang, X. *J. Phys. Chem. B* **2006**, *110*, 3964.
[20] Green, M.; Liu, F. M. *J. Phys. Chem. B* **2003**, *107*, 13015.
[21] Schroetter, H. W.; Kloeckne, H. W. In *Raman spectroscopy of gases and liquids*; Weber, A., Ed.; Springer: Berlin, 1979; p 123.
[22] Placzek, G. *Z. Physik* **1931**, *70*, 84.
[23] Neugebauer, J.; Reiher, M.; Kind, C.; Heiss, B. A. *J. Computational Chem.* **2002**, *23*, 895.
[24] Schrader, B.; Moore, D. S. *Pure and Appl. Chem.* **1997**, *69*, 1451.
[25] Hayes, W.; Loudon, R. *Scattering of Light by Crystals*; Wiley: New York, 1978.
[26] http://www.gaussian.com/.
[27] http://www.msg.ameslab.gov/GAMESS/.
[28] Boyd, R. W. *Nonlinear Optics*; Academic Press: New York, 1992.
[29] Jensen, L.; Schatz, G. C. *J. Phys. Chem. A* **2006**, *110*, 5973.
[30] Frisch, M. J. et al. *Gaussian*; Technical Report, 2003.
[31] Becke, A. D. *J. Chem. Phys.* **1993**, *98*, 5648–5652.
[32] Lee, C.; Yang, W.; Parr, R. G. *Phys. Rev. B* **1988**, *37*, 785789.
[33] Kato, Y.; Takuma, H. *J. Chem. Phys.* **1971**, *54*, 5398.
[34] Le Ru, E. C.; Meyer, M.; Etchegoin, P. G. *J. Phys. Chem. B* **2006**, *110*, 1944.

[35] Novotny, L.; Hecht, B. *Principles of nano-optics*; Cambridge University Press: Cambridge, 2006.
[36] Saleh, B. E. A.; Teich, M. C. *Fundamentals of Photonics*; John Wiley & Sons: New York, 1991.
[37] Yariv, A. *Optical Electronics*; Sunders HBJ: New York, 1991.
[38] In our system, a Jobin-Yvon LabRam, the pinhole size d actually corresponds to the length of the diagonal of the square aperture and is accordingly related to L by $d = 2\sqrt{2}L$.
[39] Suzaki, Y.; Tachibana, A. *Appl. Opt.* **1975**, *14*, 2809.
[40] Le Ru, E. C.; Etchegoin, P. G.; Meyer, M. *J. Chem. Phys.* **2006**, *125*, 204701.